Some phenomena occuring during the interaction of an electron beam with a magnetoplasma

W. Herrmann

IPP 2/61 April 1967

INSTITUT FÜR PLASMAPHYSIK

GARCHING BEI MÜNCHEN

INSTITUT FÜR PLASMAPHYSIK

GARCHING BEI MÜNCHEN

Some phenomena occuring during the interaction of an electron beam with a magnetoplasma

W. Herrmann

IPP 2/61 April 1967

Die nachstehende Arbeit wurde im Rahmen des Vertrages zwischen dem Institut für Plasmaphysik GmbH und der Europäischen Atomgemeinschaft über die Zusammenarbeit auf dem Gebiete der Plasmaphysik durchgeführt.

SOME PHENOMENA OCCURING DURING THE INTERACTION
OF AN ELECTRON BEAM WITH A MAGNETOPLASMA

Abstract

IPP 2/61 Winfried Herrmann

Some Phenomena Occuring During the Interaction of an Electron Beam with a Magnetoplasma

April 1967

Abstract

A beam of electrons penetrating a neutral gas creates a plasma with which it interacts. It is shown theoretically that oscillations with frequencies just below the upper hybrid frequency ($\omega_H^2 = \omega p^2 + \omega c^2$) will be excited. In the theory the electrostatic approximation is used, but a study is made of the conditions under which this approximation is valid. Oscillations near the upper hybrid frequency were detected experimentally. An experimental criterion for stability of the beam-plasma was deduced. With increasing density the excited oscillations lead to a turbulent state. This turbulent state of the system is characterized by high energy losses of the beam particles. The electric fields, which cause the energy losses of the beam particles are concentrated in a small region $d \lesssim 15$ cm behind the entrance slit of the beam in the plasma chamber. Increasing the interaction length does not appreciably change the losses.

A) I N T R O D U C T I O N

A beam of electrons penetrates a neutral gas and creates a plasma with which it can interact. The main phenomena observed in the beam-plasma system may be attributed to at least two states of the system, these being referred to as non-turbulent and the turbulent state. The nonturbulent state is characterized by low density, small luminosity and the original monochromatic energy distribution of the beam particles. In this state oscillations may appear which do not appreciably alter the distribution function. The turbulent state shows high density, high luminosity and substantial energy loss of the beam particles accompanied by a large broadening of the distribution function.

The particular state existing depends on the parameters of the system. The two states can best be distinguished by the neutral gas pressure. The nonturbulent state exists with low pressure, the turbulent state with high pressure. The transition between the two states is very abrupt which may be explained as follows: In the nonturbulent state oscillations are excited. The amplitude of these oscillations depends on the density of the plasma, and this density depends on the neutral gas pressure (see Chapter C IV). Increasing the pressure thus increases the amplitude of the oscillations as well. At a certain critical pressure the electrons of the plasma gain so much energy from the oscillations that additional ionization results. This increases the density, with the density the amplitude and so on until non-linear phenomena stop this escalation.
The importance of fast particles in a plasma for the occurence of self-excited waves was first pointed out by W.O. Schumann/ 1 /. J. R. Pierce / 2 / explained ion oscillations in terms of beam-plasma interaction. The basic theoretical work on multistream plasmas was performed by O. Bohm and E.P. Cross / 3 / and by A.I. Achiezer and Ya. B. Fainberg / 4 /. The experiments described in this paper were stimulated by the work of R. Kippenhahn and H.L. de Vries / 57 / and E. Canobbio and R. Croci / 58, 60, 61 / and are intended as preliminary experiments for an ion beam-plasma experiment.
The first part of this paper gives a theoretical description of the nonturbulent state. In the second part the experiments are described.

B) THEORETICAL TREATMENT OF THE BEAM-PLASMA SYSTEM

I. The most important conditions

In order to give a theoretical treatment of the beam-plasma-system, a model must be chosen. For this the following assumptions are made:

1) The system consists of two separate components: the electron beam and the plasma.
2) The system is quasi-neutral.
3) The important interactions occur between the electrons of the beam and the electrons of the plasma. The mobility of the ions is neglected $m_e/m_i = 0$.
4) The plasma is confined by an external homogeneous magnetic field $\vec{B}_o$.
5) In the zeroth approximation the beam is directed parallel to $\vec{B}_o$.
6) There is no external electric field.
7) Collisions are neglected.
8) The electrons of beam and plasma are cold.
9) The system is infinite along $\vec{B}_o$.
10) Beam and plasma are homogeneous.
11) Beam and plasma have the same diameter and fill a highly conductive metal cylinder.

The assumptions 8-11 will be discussed shortly in the following section.

II) Discussion of the conditions

a) Temperature of beam and plasma

A plasma may be regarded as cold (see also / 5 /) if $|kv_{th}| \ll |kv_\varphi|$ (k = wave number; v_{th} = mean thermal velocity of plasma electrons; $\vec{v}_\varphi$ = phase velocity). In the frequency range of interest it is found from Fig. 1 that $v_\varphi \gtrsim \frac{v_0'}{2}$ ($\vec{v}'_0$ = beam velocity). The plasma temperature inside the beam is not measured. But if we suppose that the temperature of the plasma in the immediate vicinity of the beam does not differ appreciably from the temperature in the beam region, we find from Fig. 18

$$\frac{v_{th}}{v_\varphi} \approx \frac{1}{18}$$

This means that the temperature of the plasma electrons may be regarded as cold (see also / 6 /).

The temperatures of the beam particles may be neglected / 7 / if $dv'/v_0' < \omega_p'/\omega$ or, according to / 8 /, if $u'/v_0' \ll \omega_p'/\omega_p$ where dv' is the velocity scatter of the beam particles, u' their mean thermal velocity, w_p' the plasma frequency of the beam particles ($w_p'^2 = \frac{4\pi n_p' e^2}{m}$ where n_p' is the density of the beam electrons), w_p = the plasma frequency of the plasma electrons ($\omega_p^2 = \frac{4\pi n_p e^2}{m}$, where n_p is the density of the plasma electrons), w the frequency of interest. Both conditions are deduced for the case of a plasma without magnetic field. The measurements of the beam particle velocity give an upper limit in the nonturbulent state of dv' or u', which corresponds to about 5 eV. In the turbulent state the energy scatter reaches values of 100 eV and more. Characteristic values of w'/w and w'/wp are found between 0,2 and 0,1 in the nonturbulent state and are lower than 0,1 in the turbulent state. With these values it follows that the beam may be considered cold in the nonturbulent, but not in the turbulent state.

b) Length of the system

Very few workers consider the finite length of the system in their theories. The system is normally regarded as infinite. This means that the length L is much longer than the wavelength. $L \gg \lambda$. An estimate of λ is obtained by characteristic values of w and v_φ. w is about w_c ($w_c = eB_0/mc$ = cyclotron frequency of the electrons), and $v_\varphi \lesssim v_0'$ in the region of interest. This gives

$$\frac{L}{\lambda} = \frac{L\ w_c}{2\pi v_\varphi} \gtrsim \frac{L\ w_c}{2\pi v_0'} .$$

For the standard values of the experiment B_0 = 350 gauss, U_B = 4 kV and L = 40 cm, we obtain $L/\lambda \gtrsim 10$. The system seems to be long, but may be not long enough for a convective instability to be amplified by a few orders of magnitude. Reflection of the waves at the end plate or suppression of convective instabilities have to be expected.

c) Homogeneity of beam and plasma

We suppose that beam and plasma are homogeneous in density along the magnetic field. However, the density across the magnetic field and the beam radius cannot be considered homogeneous, as figure 9 shows for the beam density. The plasma density is probably inhomogeneous as well. Weak inhomogeneities do not cause any major changes in the results, as may be found from / 11,12 /. As far as this work is concerned it would give rise to many complications if we were to attempt to consider inhomogeneous densities. These will be neglected, but we have to bear in mind that taking the inhomogeneities into account could change the results.

d) Radial limitation

In the case without turbulence the plasma density decreases very strongly outside the beam (Fig. 19). From this it seemed to be realistic to assume, that the plasma is concentrated only in the region of the beam, this is in a cylinder with a diameter $d \approx 5$ mm. Now it should be assumed that the beam-plasma region is surrounded by a vacuum and more outside by a metallic waveguide. But because experiments have shown that the diameter of the waveguide, as long as it is much larger than the diameter of the beam, had no strong influence on the main results, we assumed a model for the sake of simplicity, where the beam-plasma region directly contacts the waveguide.
Because the waves under consideration had a wavelength $\lambda \gtrsim d$, the finite diameter of the system had to be taken into account.
The results of this calculation are later compared with calculations made by GORBATENKO. His results apply to the case when beam and plasma have the same diameter but are surrounded by a vacuum /13, 14/.
The conditions under which the electrostatic approximation is valid are derived in BIV.

III) Calculation of the ε-tensor and dispersion relation

Under the conditions stated the beam-plasma system in the nonturbulent state is described by the equations of motion, the equations of continuity and the Maxwell equations. +
The system contains the unknowns: $\vec{v}$, n, $\vec{v}'$, n', $\vec{E}$, $\vec{B}$. The primed quantities refer to the beam. Since only small deviations from the equilibrium state are to be considered, we linearize as follows:

In equilibrium it holds that: $\vec{v}_0 = \vec{E}_0 = 0$.
The system of equations obtains the form:

$$m \frac{\partial \vec{v}_1}{\partial t} = -e\left\{\vec{E}_1 + \frac{1}{c}\left[\vec{v}_1 \times \vec{B}_0\right]\right\} \tag{1}$$

$$m\left(\frac{\partial \vec{v}_1'}{\partial t} + \vec{v}_0' \frac{\partial \vec{v}_1'}{\partial z}\right) = -e\left\{\vec{E}_1 + \frac{1}{c}\left[\vec{v}_0' \times \vec{B}_1\right] + \frac{1}{c}\left[\vec{v}_1' \times \vec{B}_1\right]\right\} \tag{2}$$

$$\operatorname{div}\left(n_0' \vec{v}_1' + n_1' \vec{v}_0'\right) = -\frac{\partial n_1'}{\partial t} \tag{3}$$

$$\vec{j}_1 = -e\left(n_0 \vec{v}_1 + n_0' \vec{v}_1' + n_1' \vec{v}_0'\right) \tag{4}$$

$$\operatorname{curl} \vec{E}_1 = -\frac{1}{c} \frac{\partial \vec{B}_1}{\partial t} \tag{5}$$

$$\operatorname{curl} \vec{B}_1 = \frac{1}{c} \frac{\partial \vec{E}_1}{\partial t} + \frac{4\pi}{c} \vec{j}_1 \tag{6}$$

+Calculations with temperature in quasi-electrostatic approximation are described in /15, 16/; with temperature in general coordinates for $[v_0' \times B_1] \ll E_1$ in -/17/; the same without temperature with damping in /18/; without temperature quasi-electrostatically for various configurations in /19/; in detail for infinitely strong magnetic fields in /20/.

The magnetic field produced by the current $\vec{j}_0$ is neglected in eqs. (1) and (2). For the present system of equations it was assumed that the directions of beam and magnetic field coincide in the zeroth approximation, and that this direction fixes the z-axis of a coordinate system. Cylindrical coordinates are used as follows.

Solutions in the form of cylindrical waves are required for the system of equations (1) to (6). The following assumption is therefore made for all values:

$$q_1 = q(r)\, e^{-i(\omega t - l\varphi - kz)} \tag{7}$$

Eqs. (5) and (6) can be combined:

$$\operatorname{curl}\operatorname{curl}\vec{E}_1 = -\frac{1}{c^2}\frac{\partial^2 \vec{E}_1}{\partial t^2} - \frac{4\pi}{c^2}\frac{\partial \vec{j}_1}{\partial t}$$

Together with (7) this gives:

$$\operatorname{curl}\operatorname{curl}\vec{E}_1 = \frac{\omega^2}{c^2}\left(\vec{E}_1 + \frac{4\pi i}{\omega}\vec{j}_1\right) \tag{8}$$

With the aid of (1), (2), (3), (5) $\vec{j}_1$ can be expressed as a function of $\vec{E}_1$ in the form:

$$\vec{j}_1 = \overleftrightarrow{\sigma}\,\vec{E}_1 \tag{9}$$

Substituting (9) in (8) gives:

$$\operatorname{curl}\operatorname{curl}\vec{E}_1 = \frac{\omega^2}{c^2}\left(\overleftrightarrow{1} + \frac{4\pi i\overleftrightarrow{\sigma}}{\omega}\right)\vec{E}_1 \tag{10}$$

With the abbreviation:

$$\overleftrightarrow{\varepsilon} = \overleftrightarrow{1} + \frac{4\pi i\overleftrightarrow{\sigma}}{\omega}$$

(10) becomes

$$\operatorname{curl}\operatorname{curl}\vec{E}_1 = \frac{\omega^2}{c^2}\overleftrightarrow{\varepsilon}\,\vec{E}_1 \tag{11}$$

$\overleftrightarrow{\varepsilon}$ being the dielectric tensor. Eq. (11) is the solution for $\vec{E}_1$. Once $\vec{E}_1$ is found, all the other values of eqs. (1) to (6) can be obtained.

With the aid of (7) the dielectric tensor can be obtained from eqs. (1), (2), (3) and (5). Though roundabout, this method is nevertheless easy to follow. The dielectric tensor is written here as the sum of two tensors $\overleftrightarrow{\varepsilon}_0$ and $\overleftrightarrow{\varepsilon}_1$. The tensor $\overleftrightarrow{\varepsilon}_0$ is obtained by neglecting the term $\frac{1}{c}[\vec{v}_0' \times \vec{B}_1]$ in (2). The tensor $\overleftrightarrow{\varepsilon}_1$ contains the correction terms for $\frac{1}{c}[\vec{v}_0' \times \vec{B}_1] \neq 0$

$$\begin{vmatrix} 1-Q-P\frac{\bar{\omega}}{\omega} & (Q+P)\frac{\omega_c}{\omega}i & 0 \\ -(Q+P)\frac{\omega_c}{\omega}i & 1-Q-P\cdot\frac{\bar{\omega}}{\omega} & 0 \\ \frac{P v_0'}{\omega}\left(\frac{i}{r}\frac{\partial}{\partial r}r\ldots + i\frac{l}{r}\frac{\omega_c}{\bar{\omega}}\right) & \frac{P v_0'}{\omega}\left(\frac{\omega_c}{\bar{\omega}}\frac{1}{r}\frac{\partial}{\partial r}r\ldots - \frac{l}{r}\right) & 1-\frac{\omega_p^2}{\omega^2}-\frac{\omega_p'^2}{\bar{\omega}^2} \end{vmatrix} = \overleftrightarrow{\varepsilon}_0 \tag{12}$$

$$\begin{vmatrix} \frac{P\bar{\omega}k v_0'}{\omega^2} & -\frac{P\omega_c k v_0'}{\omega^2}i & \frac{P v_0'}{\omega^2}i\left(\bar{\omega}\frac{\partial}{\partial r}\ldots + \frac{\omega_c l}{r}\right) \\ \frac{P\omega_c k v_0'}{\omega^2}i & \frac{P\bar{\omega}k v_0'}{\omega^2} & -\frac{P v_0'}{\omega^2}\left(\omega_c\frac{\partial}{\partial r}\ldots + \frac{\bar{\omega}l}{r}\right) \\ -\frac{P k v_0'^2}{\omega^2}\left(\frac{1}{r}\frac{\partial}{\partial r}r\ldots + \frac{\omega_c l}{\bar{\omega}r}\right)i & -\frac{P k v_0'^2}{\omega^2}\left(\frac{\omega_c}{r\bar{\omega}}\frac{\partial}{\partial r}r\ldots - \frac{l}{r}\right) & \frac{P v_0'^2}{\omega^2}\Delta_r\ldots - \frac{P v_0'^2 l^2}{\omega^2 r^2} \end{vmatrix} = \overleftrightarrow{\varepsilon}_1 \tag{13}$$

where

$$Q = \frac{\omega_p^2}{\omega^2 - \omega_c^2} \qquad P = \frac{\omega_p'^2}{\bar{\omega}^2 - \omega_c^2}$$

$$\omega_p^2 = \frac{4\pi n_0 e^2}{m} \qquad \omega_p'^2 = \frac{4\pi n_0' e^2}{m}$$

$$\bar{\omega} = \omega - k v_0 \qquad \omega_c = \frac{e B_0}{m \cdot c} \qquad \Delta_r = \frac{1}{r}\frac{\partial}{\partial r} r \frac{\partial}{\partial r}$$

The $\vec{\vec{\epsilon}}$ tensor is an operator and complicates eq. (11). Eqs. (12) and (13) do not show, however, why the terms of (13) could be neglected in relation to the corresponding terms of (12), i.e. why we could set $|\vec{v}_0' \times \vec{B}_1| \ll |\vec{v}_1' \times \vec{B}_0|$ as in /19, 18/ for instance. In general, this is certainly not correct. For the Cerenkov effect, for example, the factor kv_0'/w, by which most beam terms in $\vec{\vec{\epsilon}}_0$ and $\vec{\vec{\epsilon}}_1$ differ, is of the order of 1. Since, however, general solutions cannot be obtained with the calculated $\vec{\vec{\epsilon}}$ tensor, we shall only look for solutions in the electrostatic approximation. The conditions under which the electrostatic approximation is valid will then be discussed in section B IV.

Subsequently the equation

$$\operatorname{div} \vec{\vec{\epsilon}} \vec{E}_1 = 0 \quad {}^{+} \tag{14}$$

will be investigated with the ansatz:

$$\vec{E}_1 = - \operatorname{grad} \phi_1 \tag{15}$$

If, in addition, we set $l = 0$, i.e. all values do not depend on φ, (14) together with (15) and (12) gives the familiar /21/ differential equation for the potential:

$$\Delta_r \phi_1 = \frac{\vec{\vec{\epsilon}}_3'}{\vec{\vec{\epsilon}}_1'} k^2 \phi_1 \tag{16}$$

$$\left.\begin{aligned} \vec{\vec{\epsilon}}_1' &= 1 - Q - P \\ \vec{\vec{\epsilon}}_3' &= \vec{\vec{\epsilon}}_{033} = 1 - \frac{\omega_p^2}{\omega^2} - \frac{\omega_p'^2}{\bar{\omega}^2} \end{aligned}\right\} \tag{17}$$

The solution for ϕ_1 is subject to the condition that the waveguide is uniformly filled by beam and plasma and that the potential on the axis is finite:

$$\phi_1 = J_0(T \cdot r) \cdot e^{-i(\omega t - kz)}$$

Provided that the potential at the boundary vanishes for $r = R$, we obtain a condition for T which represents the dispersion relation at the same time:

$$T \cdot R = p_{0\nu}$$

$p_{0\nu}$ are the zeros of the Bessel function I_0. For the fundamental mode we have:

$$p_{0\nu} = 2.4$$

T is given by

$$T = \sqrt{- \frac{\vec{\vec{\epsilon}}_3'}{\vec{\vec{\epsilon}}_1'}} \cdot k$$

+ The equations $\operatorname{div} \vec{\vec{\epsilon}} \vec{E}_1 = 0$ and $\operatorname{div} \vec{\vec{\epsilon}}_0 \vec{E}_1 = 0$ give the same result with $\vec{E}_1 = - \operatorname{grad} \phi_1$.

For the fundamental mode the dispersion relation is thus as follows:

$$\frac{2{,}4}{R} = \sqrt{-\frac{\varepsilon_z'}{\varepsilon_r'}}\cdot k \tag{18}$$

where R is the beam radius.
This equation was solved for w and all frequencies normalized to w_c.

IV) Validity of the electrostatic approximation

Before turning to the dispersion relation, let us investigate the conditions under which the electrostatic approximation is valid. For this purpose $c\,\mathrm{curl}\,\vec{B}_1$ has to vanish.

$$c\,\mathrm{curl}_r \vec{B}_1 = -\frac{i\omega}{c}\left(\varepsilon_{0rr} E_{1r}\right) = 0$$

$$c\,\mathrm{curl}_\varphi \vec{B}_1 = -\frac{i\omega}{c}\left(\varepsilon_{0r\varphi} E_{1r}\right) = 0 \tag{19}$$

$$c\,\mathrm{curl}_z \vec{B}_1 = \frac{\omega_p'^2 \cdot v_0'}{(\bar{\omega}^2-\omega_c^2)\cdot c}\cdot\frac{1}{r}\frac{\partial}{\partial r} r E_{1r} - \frac{i\omega}{c}\left(\varepsilon_{0zz} E_{1z}\right) = 0$$

These simple expressions are valid provided that:

$$c\,\mathrm{curl}\,\vec{E}_1 = 0$$
$$\frac{\partial}{\partial\varphi} = 0 \tag{20}$$

Since $E_{1r} = 0$ leads to the trivial solution $\vec{E}_1 \equiv 0$, we are left with

$$\varepsilon_{orr} = 0$$
$$\varepsilon_{or\varphi} = 0$$

The third equation (19) can be written with (20) in the form:

$$\Delta_r E_{1z} + \frac{\varepsilon_{0zz}}{\frac{\omega_p'^2\cdot k\cdot v_0'}{\omega(\bar{\omega}^2-\omega_c^2)}}\cdot k^2 E_{1z} = 0 \tag{21}$$

Comparing (21) with (16) shows that (21) is satisfied on condition that:

$$\varepsilon_1' = -\frac{\omega_p'^2 k v_0'}{\omega(\bar{\omega}^2-\omega_c^2)}$$

ε_1' is given by (17).
As can easily be checked, this equation is identically satisfied for $\varepsilon_{orr} = 0$.
Subject to the conditions $\varepsilon_{or\varphi} = 0$ and $\omega_p'^2 \ll \omega_c^2$ it follows from the equation $\varepsilon_{orr} = 0$ that

$$k v_0' \approx \omega \pm \omega_c - \frac{\omega_p'^2}{2\omega} \tag{22}$$

That is, $c\,\mathrm{curl}\,\vec{B}_1$ is small when $\omega - k v_0'$ is in the vicinity of w_c, i.e. the electrostatic approximation is valid for the anomalous Doppler effect.
From the equation $\varepsilon_{or\varphi} = 0$ taken with (22) it follows that:

$$\omega \approx \sqrt{\omega_c^2+\omega_p^2} + \frac{\omega_c\omega_p^2 - \omega_p^2\sqrt{\omega_c^2+\omega_p^2}}{2\omega_c^2+3\omega_p^2} \tag{23}$$

Under the experimental conditions the second term on the right-hand side is small and always negative.
Since (22) and (23) have to be satisfied jointly, it follows that the electrostatic approximation yields exact results in the vicinity of the anomalous Doppler effect and at frequencies just below the upper hybrid frequency. If it is desired to make a check for a pair w and k from the dispersion relation obtained quasi-electrostatically to see whether these corr espond with the general

equation, this is done best by substituting ω and k in ε_{orr} and $\varepsilon_{o\tau\varphi}$ and verifying whether

$$|\varepsilon_{orr}| \ll 1 \qquad \text{and} \qquad |\varepsilon_{o\tau\varphi}| \ll 1 \tag{24}$$

For small frequencies ω for which $\left|\frac{\omega^2}{c^2}\right| \ll \frac{1}{S'^2}$ it is sufficient for the solution to be valid that

$$|\varepsilon_{o\tau\varphi}| \lesssim 1 \quad , \quad |\varepsilon_{orr}| \lesssim 1 \tag{25}$$

S is some characteristic length for the change of $\vec{B}_o$. For the basic mode considered, S is of the order of the diameter of the beam.

V) Discussion of the dispersion relation

a) General remarks

Eq. (18) gave the dispersion relation for the quasi-electrostatic system subject to the condition that the system is rotation symmetric, that plasma and beam have the same diameter and, in addition, are bounded by a metal wall.
Eq. (18) was numerically solved for various values. Fig. 1 shows one result. The plot is made on the abscissa ω/ω_c as a function of the ordinate kv_o'/ω_c. The curves in the upper quadrant can virtually be reproduced by six straight lines. These six lines represent the waves that are possible in beam and plasma separately. The two lines designated as the "plasma wave" and "cyclotron wave" belong to the plasma. They also occur without a beam /22, 23, 24, 25/. The other four lines, designated as the fast and slow plasma waves and the fast and slow cyclotron waves, are waves in the beam which occur without plasma. Such dispersion diagrams have already been discussed often enough (e.g./22/) and will not be dealt with in any greater detail here. The circles enclosing the letters A,B, C refer to regions where the frequencies and phases of waves in the beam and plasma agree. Energy exchange can take place in these regions. This is indicated by an imaginary part of the frequency ω. If $\mathrm{Im}(\omega) > 0$ the wave amplitude increases.

The interaction in the region A will not be investigated further here. In connection with the experiments described later we are primarily interested here in the regions B and C. For both regions the conditions for the quasi-electrostatic approximation prove to be tolerably satisfying.
The region B refers to the interaction of the plasma wave in the beam with the cyclotron wave in the plasma. The phase velocity of the waves is near the beam velocity. For real k, ω is complex in this region (k is also complex for real ω. Subsequently, however, only the imaginary part of ω is dealt with).
Only complicated calculation /27, 28/ can determine whether the instability in B is convective or absolute. The condition that the phase velocity of the wave is equal to the beam velocity,

$$\omega \approx kv_o'$$

is no other than that for the Cerenkov effect.
The interaction in the region C occurs when $\omega+\omega_c \approx kv_o'$ is satisfied. This is the condition for the anomalous Doppler effect, which leads to instability on interaction of the slow cyclotron wave in the beam with the cyclotron wave of the plasma. Since ω is not much greater than ω_c, the phase velocity is about half the beam velocity. In the region C there is only one growth rate with time, i.e. complex ω for real k. According to /28/ this signifies an absolute instability. This statement, however, is valid in the last resort only for infinitely extended plasma. In a finite system the instability condition may easily depend

on the length.

b) Growth rates

The size of the growth rate indicates which interaction really occurs. The maximum of the imaginary part of ω and the relevant real part for real k were determined numerically. Fig. 2 shows the two growth rates as a function of the product of the magnetic field and radius: rB, for fixed $\Omega = \omega_p/\omega_c$ and constant beam current I_B! The growth rates are normalized to ω_c. It can be seen that in the case of large rB the interaction of the plasma wave with the cyclotron wave (Cerenkov effect) predominates. For small rB the anomalous Doppler effect prevails /29/. As the plasma density increases (Fig. 3) so do the two imaginary parts, the growth rate for the Doppler effect more than that for the Cerenkov effect. It can be expected that the growth rate as a function of the magnetic field shifts with increasing density in favour of the anomalous Doppler effect, i.e. the intersection of the curves in Fig. 2 is expected with increasing density for a higher magnetic field.

The growth rates also vary appreciably as a function of the beam radius and the radial mode number. In Fig. 4 the growth rate is plotted as a function of $r/p_{0\nu}$. The plasma density and beam density are thereby assumed to be constant. For a small radius and waves of high radial wave number the anomalous Doppler effect clearly predominates. If the radius decreases or the radial wave number increases, the region of the magnetic field (Fig. 2) for which the anomalous Doppler effect predominates is further extended.

From Fig. 2 it can also be seen that for small magnetic fields it holds approximately for the region C that

$$\frac{\omega_i}{\omega_c} \approx \frac{M'}{\omega_c}$$

i.e. the growth rate practically does not depend on the magnetic field for constant ω_p/ω_c.

c) Interaction frequencies

For small rB the frequencies of both instabilities approach the upper hybrid frequency ω_H (Fig. 5) ($\omega_H^2 = \omega_p^2 + \omega_c^2$). For small radii and small magnetic fields only slight deviations of the frequency from ω_H should be expected, mainly for the Doppler effect.

VI) Comparison with results of GORBATENKO

GORBATENKO /14/ calculates the excitation of waves in a beam plasma subject to the conditions that the beam and plasma have the same small diameter and are surrounded by a vacuum. The calculation is not restricted to the quasi-electrostatic case. But it is postulated that

$$k \cdot R \ll 1$$

Since k cannot become arbitrarily small (k is approximately determined by the beam velocity and frequency), the inequality signifies that the results are only valid for very small beam diameters R. The other conditions are the same as those given on page 3 .

For the anomalous Doppler effect GORBATENKO obtains a maximum growthrate:

$$\mathrm{Im}(\omega)_{max} = \frac{\omega_p'}{2}\sqrt{\frac{\omega_+(\omega_+^2 - \omega_c^2)}{\omega_c(\omega_+^2 - \omega_-^2)}} \qquad (26)$$

ω_+ is the interaction frequency and is given by:

$$\omega_+^2 = \omega_H^2 - \omega_-^2 = \omega_c^2 + \omega_p^2 - \omega_-^2$$

with $$\omega_- = \frac{\omega_e^2 \omega_p^2 k^2 R^2}{\lambda_p^2 \cdot \omega_H^2}$$

(The quantity λ_p is not exactly defined by GORBATENKO. It seems, however, to have a value between 2.4 and 5.5) If $kR \ll 1$ then $\omega_-^2 \ll \omega_H^2$ and (26) can be written:

$$\mathrm{Im}(\omega)_{max} = \frac{\omega_p'}{2}\sqrt{\frac{\omega_H \omega_p^2}{\omega_c \cdot \omega_H^2}} = \frac{\omega_p'}{2}\sqrt{\frac{\omega_p^2}{\omega_c^2}} \cdot \frac{1}{\sqrt{1 + \frac{\omega_p^2}{\omega_c^2}}} \qquad (27)$$

It can be seen that the growth rate is now only a function of the beam density and the ratio of ω_p and ω_c. For a constant ratio ω_p/ω_c the growth rate depends neither on the magnetic field nor on the plasma density.
The deviation of the frequency ω from ω_H is given by $\Delta\omega = \omega_-$ and is small for small radius and low density, but increases with the magnetic field when the ratio of the plasma frequency to the cyclotron frequency is constant.
For the Cerenkov effect GORBATENKO calculates the same frequency and a growth rate which- on the assumption that $\omega_-^2 \ll \omega_H^2$-, is written:

$$\mathrm{Im}(\omega)_{max} = \frac{\sqrt{3}}{2^{4/3}} \cdot \left[\frac{k^2 R^2 \omega_p'^2 \cdot \omega_p^2}{\lambda_p^2 \cdot \omega_H} \right]^{1/3}$$

The growth rate increases with the radius and beam density. If $\omega_p \ll \omega_c$, the growth rate increases in proportion with ω_c for constant ω_p/ω_c.
Qualitatively, the results of GORBATENKO agree very closely with ours for $kR \ll 1$. For $kR \gtrsim 1$ they give no longer any information.

VII) Influence of damping processes

For the anomalous Doppler effect and the Cerenkov effect both calculations give for all ω_p and ω_p' positive imaginary parts of ω. In other words, it should be possible to find oscillations in the region $\omega \approx \omega_H$ for every plasma density. Experimentally, this is not the case, however, because of damping processes. These are Landau damping and collision damping. Self-excited oscillations can only occur when the growth rate ω_i is greater than the damping rate ω_D.

If it is assumed that the damping rate hardly depends on the plasma density and magnetic field, it is possible to arrive at a more far-reaching conclusion for the anomalous Doppler effect. The growth rate in this case is a monotonically increasing function of ω_p/ω_c:

$$\omega_i = f_{max}\left(\frac{\omega_p}{\omega_c}\right); \quad \frac{df}{d\left(\frac{\omega_p}{\omega_c}\right)} > 0$$

If we then have $\omega_i > \omega_D = \text{const}$, it follows that:
oscillations can occur for the case

$$\frac{\omega_p}{\omega_c} > \left(\frac{\omega_p}{\omega_c}\right)_{crit.}$$

i.e. oscillations can occur if a certain ratio of the plasma frequency to the cyclotron frequency is exceeded.

C) EXPERIMENTAL INVESTIGATION

I) Apparatus

An apparatus previously constructed for a hot cathode PIG discharge was used for the electron beam interaction experiment. Additions in the form of a stainless-steel container with electron gun and measuring equipment were made to this existing device. Fig. 6 gives a sketch of the apparatus.

a) Electron gun

The beam was accelerated in two stages from a nickelous oxide cathode in a protective cage. The first electrode controlled the beam current by means of the accelerating voltage, the second provided acceleration to the desired voltage. The other two electrodes served at first to keep away ions and electrons coming from the plasma. Since, however, potential at these electrodes caused oscillations, they were later grounded or removed altogether. The nickelous oxide cathode was later replaced by tantalum cathode because the oxide layer was destroyed by ion sputtering. The electron gun was suspended with the accelerating electrodes from the roof of the container. It was also possible to shift the gun during operation and, in this way, to direct the beam through the diaphragm.
The vessel with the electron gun was evacuated by two pumps of type DO-121. Even when the pressure in the plasma container was increased till sometimes 10^{-3} torr, the pressure in the accelerating system did not rise appreciably above 10^{-5} torr.

b) Plasma chamber

The electron beam reaches the plasma chamber through a cooled diaphragm 12 mm long and 5 mm in diameter. The diaphragm acts as a pressure stage. The vessel of the plasma chamber consists of two glass tubes separated from one another by a bronze ring. The bronze ring contains a few windows, the gas inlet, a pump connection, the pressure gauge and a few ducts for probes or other instrument leads. The mean diameter of the vessel was 150 mm, the total length being 56 cm. The bottom cover could be shifted horizontally like the top one. In addition, it had a retaining ring duct 50 mm in diameter through which probes, targets or even the retarding field could be passed and moved parallel to the axis. The base pressure in the container was 10^{-5} torr.

The entire plasma container was located in a magnetic field produced in a set of individual coils. Only in the region of the two closely packed coils on the outside was the magnetic field inhomogeneous. In the remaining part the deviations from homogeneity were smaller than 1%. It was possible in continuous operation to attain maximum fields of 1200 gauss. At a current of 1 A the field on the axis was 5 gauss. Up to 70 A (350 gauss) the current was supplied by 12 V accumulators. For higher currents a generator was used. Since, however, the generator was subject to slow and fast fluctuations, most experiments were conducted at 350 gauss.

c) Retarding field analyser

The retarding field configuration is one of the main pieces of measuring equipment and should therefore be described as well. It forms a closed system linked to the plasma chamber by only the diaphragm aperture 0.5 mm in diameter. Through this diaphragm passes the fraction of the beam to be analysed (about 1%) and enters the retarding field apparatus. This 0.5 mm bore extends for 2.5 mm and then for a length of 10 mm the diameter is 1 mm.

The analyser system comprised four electrodes. The first, in the beam direction, had positive potential to repel the plasma ions. The second was at retarding potential, the third was mostly grounded and the target positively biased.
The entire retarding field was still located in the magnetic field. The beam thus remained on the axis of the system. Lens errors were slight. With this analyser it was possible to measure the distribution of the parallel energy of the beam electrons (parallel to the magnetic field). The retarding field container was evacuated with a diffusion pump Do 121. At high pressure in the plasma chamber (2×10^{-3} torr) the vacuum above the pump was less than 10^{-5} torr.

II) The two states of the system

a) General description of the phenomena

At the beginning of the experiment at low pressure the current and voltage of the electron beam were set. The voltage of the beam (and hence the velocity of the beam particles) was determined with a potentiometer directly from the potential of the hot cathode of the electron gun. The generator current was always taken as beam current. Standard values were usually set: for the accelerating voltage $U_B = 4$ kV, for the beam current $I_B = 50$ mA, for the magnetic field B = 350 gauss, for the length of the interaction path L = 40 cm, working gas: argon, The beam diameter is dependent on these parameters. The probable mean value was always taken as d = 0.4 cm.
At a residual gas pressure of 10^{-5} torr, the luminous column of the beam can only be made out in the dark. This column indicates approximately the diameter of the electron beam. If the pressure of the working gas (hydrogen or argon) is raised, the luminous density of the column increased slightly due to the greater number of collisions, the diameter remaining constant. This continues until a critical pressure is reached in the region of a few 10^{-4} torr, whereupon the diameter and intensity of the luminous column suddenly grow to much larger values: The system has gone from one state (called state I) to another state (called state II). As described later on, the plasma density in the vicinity of the beam and the energy distribution of the beam electrons also undergo a sudden change when the critical pressure is exceeded. Indeed, we are of the opinion that the energy distribution function of the beam electrons, though more complicated to determine, is the surest criterion of whether the discharge has changed from the state I to a state II.

Collision processes cannot be the cause of the sudden, marked change because both the excitation function and the ionization function depend steadily on the pressure. It is more likely that the beam excites in the plasma one of the instabilities described in section B, beam energy being converted in the process into wave energy and wave energy into excitation and ionization of particles. Without going into the matter in greater detail at this point, we shall therefore refer to the state I as the nonturbulent state, to state II as the turbulent state and to the critical pressure p_{crit} as the pressure denoting the start of turbulence.

The sudden transition from state I to II was first described by /30, 31/. It has also been observed by other authors /22, 32, 33, 34/, though often only in the form of a perturbation during density or frequency measurements /35/. The measurements of /30/ will be discussed in the following chapter.

b) The limits between the two states, or the region of existence of the beam plasma turbulence

The critical pressure p_{crit} is not a constant but depends on the parameters of the system. In Figs. 7a to 8b it is given as a function of the beam current, beam voltage and length of the beam path in the plasma. With rising beam current (Fig. 7a) the critical pressure

drops, with increasing voltage (Fig. 7b) it rises. If the length of the interaction path decreases (Fig. 8b) it increases. The critical pressure does not vary monotonically with the magnetic field (Fig. 8a). Fig. 8a also conveys an idea of the reproducibility of the measurements.

In the measurements it was attempted to keep all the parameters used for the series constant. This was difficult in the case of the beam radius and hence of the beam density as well. In the investigations with the retarding field, measurements were also always made to check the zero setting in the stable region. From these measurements it can be seen that the beam current density increases almost in proportion to the current strength.

From the calculations (27) and from Fig. 3 it can be seen that for the growth rate in the anomalous Doppler effect we obtain for $\omega_p < \omega_c$:

$$\omega_i \approx \omega_p' \cdot \omega_p^{1/2}$$

According to a simple diffusion theory /36/ (see Appendix A) it can be assumed that the density of the plasma in the region of the beam increases in proportion to the beam density and to the square of the neutral gas pressure (see Appendix A, eq. (31)). This gives:

$$\omega_i \propto \omega_p'^{3/2} \cdot p_{eff}^{1/2} \approx n_p'^{3/4} \cdot p_{eff}^{1/2}$$

where $p_{eff} = p - p_o$. This p_o can be imagined as the pressure required to neutralize the electron beam. It depends on the type of gas and on impurities. As the instability will always occur under otherwise equal conditions when ω_1 reaches a critical value, it follows that:

$$\omega_i = \omega_{i\,crit} = const = n_p'^{3/4} \cdot (p_{crit} - p_o)^{1/2}$$

or

$$p_{crit} - p_o \approx \frac{1}{n_p'^{3/2}} \propto \frac{1}{J_B^{3/2}}$$

if U_B is constant. This behaviour is clearly demonstrated in Fig. 7a. The value obtained for p_o is between 6 and 8 x 10^{-5} torr, which is a very reasonable pressure for neutralizing the beam.

Similar considerations also account for the dependence of the critical pressure on the accelerating voltage. As the voltage increases, the beam density and the ionization constant decrease. At higher voltages the critical pressure therefore has to be greater for constant ω_i. The dependence on the magnetic field cannot readily be explained. When length changes, the beam radius and the beam density certainly do not vary. The maximum plasma density, on the other hand, increases with the length (see Appendix A, eq. (31)). It thus follows that:

$$\omega_i \approx \sqrt{(L + 2L_y)(p - p_o)}$$

or

$$(p_{crit} - p_o) \approx \frac{1}{L + 2L_y}$$

For lengths between 20 and 50 cm we obtain p_o = 4 x 10^{-5} torr, and L_y = 8.5 cm. These values are only rough estimates because we have to assume that p_o is dependent on L.

An estimate of the errors in Figs. 7 and 8 shows that the error of observation is small; this is indicated at several points by vertical strokes. Each experimental point is the mean of three measurements made directly after one another. The experimental error therefore offers no

information on the reproducibility. In the case of a slightly contaminated gas or other beam density profile the experimental points may easily be displaced by 10 % (see the measurements in Fig. 8a).

The arrows in Fig. 7a signify that the occurrence of instabilities in this region was not stationary, but periodic.with a very low frequency of some cycles per second. With rising pressure the frequency increased, and at the pressure marked by the top end of the arrow the repetition frequency of the turbulent state reached such a value, that the turbulent state seemed to be stationary.
Instead of a critical pressure it is, of course, possible to introduce a critical current, a critical velocity or a critical length. Measurements on the region of existence of the instability at fixed pressure and beam current have been published by the group centred round KHARCHENKO and FAINBERG /30, 37/. These authors show, for example, that for a fixed accelerating voltage there are one/30/ or several /37/ narrow regions of the magnetic field separated from one another in which the system is unstable. A few important parameters were unfortunately not given and, what is more important, there was no mention of what criterion for instability was used. In the range covered by our measurements such regions of instability bounded on both sides do not occur or else only for very short lengths ($L \approx 10$ cm). With normal parameters the system remained unstable for all pressures above the critical pressure. With very short lengths (about 10 cm) the intensified luminosity disappeared on occasion when the pressure increased, reappearing at higher pressures.

The critical pressure was always determined by pressure increase. Conversely, if pressure is reduced and the critical pressure is taken as the pressure at which the turbulence is eliminated, one obtains values which, for small magnetic fields with large lengths, are half as high as those given in Figs. 7a to 8b. The instability thus shows pronounced hysteresis.

III) Behaviour of the electron beam

The maximum beam diameter $2r_{max}$ is equal to the diameter of the opening in the entry diaphragm d = 5 mm. Since the magnetic field in this region is still inhomogeneous, the beam diamter will be smaller in the centre of the system than in the diaphragm. To all appearances the diameter does not become less than 2 mm. If it is assumed that the beam density is homogeneous over the diameter, the density n' obtained for standard values I_B = 50 mA, U_B = 4 kV is:

$$4.2 \times 10^8 < n' < 2.6 \times 10^9 \ [cm^{-3}]$$

The probable mean value obtained for r = 2 mm is

$$n' = 6.6 \times 10^8 \ [cm^{-3}]$$

The numerical calculations were made with the standard value r = o.2 cm.
The beam density profile was investigated with the retarding field analyser. The current through its diaphragm aperture o.5 mm in diameter was measured as a function of the radius with a retarding field of 1.35 kV. This retarding field ensured that no plasma electrons reached the collector.
The measurements demonstrate that the beam density is not at all homogeneous. Most of the curves show a minimum of the beam density in the centre and a maximum towards the boundary of the beam. The maxima at the boundary are by no means always equal on both sides. An example is provided in Fig. 9. The inequalities are not very pronounced here. The fluctuations

in the density profile of the beam are probably much greater than those in the curves because the experimental points represent in each case mean values over a circular area 0.5 mm in diameter. At the beam boundary the density drops almost exponentially.
If the boundary of the beam is defined as that value at which the density drops to 1 % of the maximum density and the corresponding diameter is plotted as a function of the pressure for various magnetic fields, the following qualitative statements can be obtained from many measurements of this kind:

1) With increasing magnetic field the diameter decreases.
2) In the unstable state the diameter decreases with increasing pressure.
3) Just above the critical pressure the beam diameter attains a maximum . With small magnetic fields the beam expansion attains a factor of 2.

(The diameter of the expanded beam is not identical with the diameter of the highly luminous column. The latter is still a good deal larger. For comparison see Fig. 20).

The beam density is not only a function of the radius, but also a function of the beam length. Due to the extraction (the extraction electrode acts as a lens) the space charges in the beam and the inhomogeneous magnetic field, the electrons of the beam have a radial component on entering the plasma chamber. The electrons describe spiral paths which are of equal pitch, but of periodically varying width. There are nodes and antinodes and the distance a between the nodes is given by

$$a = \frac{v_z'}{\nu_{ec}}$$

where ν_{ec} = Larmor frequency of the electrons, v_z' = beam velocity in the direction parallel to the magnetic field. In the vicinity of the standard conditions, a is of the order of centimetres. As far as could be ascertained visually, a corresponded to the pitch of the electron orbits calculated from the magnetic field and accelerating voltage. What is more, it was possible to ascertain that this distance was the same all along the beam. This means that with a homogeneous magnetic field the velocity of the electrons along the beam remains the same. This observation is not compatible with the formation of a virtual cathode, which, according to NEZLIN /98, 99, 100/ is supposed to be the cause of the instability. The formation of a virtual cathode should cause the node separations to decrease towards the centre of the beam.
The term "beam density" as used in this work refers to the density resulting when a cylinder of radius r is filled uniformly. It should be borne in mind that the local density may be considerably larger.

IV) Excited frequencies in the stable state

As the theoretical study in Chapter A shows, the beam-plasma system is unstable for practically all densities and magnetic fields. Oscillations should therefore be expected at low pressures as well. There are two reasons that contradict these predictions. The first is that there is always damping in a plasma. As long as the damping rate is higher than the growth rate no oscillations are excited. Because the growth rate increases with density, only above a density n_D, defined by the damping rate, oscillations can be expected. The second reason is that for low pressures the beam is not neutralized, and so we have electric fields. This collects the ions and quickly forces the electrons to the walls. We thus have no electron plasma and no electron oscillations. Only above a neutralizing pressure p_o do we have a plasma. It is then possible to have oscillations as well.
Both reasons together state that we can expect oscillations only in the pressure region well above $p_D + p_o$. The value p_o was found (from Fig. 8b) to be higher than 4×10^{-5} torr. We shall

therefore certainly not find oscillations below 4×10^{-5} torr. Accordingly, electron oscillations were detected only at pressures higher than 7×10^{-5} torr.
The excitation of electron oscillations may be ascribed to those values of frequency and wavelength that lie in the regions marked A, B, C in Fig. 1. All three interactions may occur simultaneously. The oscillation that finally prevails depends first of all on the growth rate. Probably, however, the finite length of the system also has some influence - in the case of absolute instabilities /38/ as well.
According to /28/ the oscillation in region A is convective, that in C absolute. The oscillation in region B cannot be discussed in terms of the curves of /28/. According to /39/, however, the investigation of absolute and convective instabilities does not play a very important role in a system of finite length because the convective waves are reflected at the end plates. Waves of both convective and absolute instabilities may occur with finite amplitude. In the case of absolute instabilities this is due to non-linear effects. For example, the amplitude of the oscillation is also determined by the number n_1 of particles involved in the oscillation. In the linear theory, however, it is postulated that $n_1 \ll n_o$. At small densities n_o the amplitude may thus be limited by non-linear effects at very low values n_1.

It was possible to pick up the oscillations in the beam with a probe placed in the vicinity of the beam and investigate them with the "Panoramic SPA-4a" spectral analyser. The probe consisted of a RF cable with its core projecting about 1 cm from the end of the cable. The probe was only a few centimetres away from the target. The oscillations had a maximum amplitude in the vicinity of the target.
The probe and cable could not be connected to the spectral analyser with complete suppression of reflections. This gave rise to interferences. With the cable lengths and connections used the frequency differences for maximum amplitude were between 30 and 120 Mc/s. These reflections are also the cause of the step-by-step growth of the frequency, as described in /40/.
Only in a narrow pressure range below the critical pressure could oscillations with a band width of less than 50 Mc/s be detected. The frequency, maximum amplitude and band width of this oscillation increased with the pressure until the oscillation changed into a general, broad noise spectrum at the critical pressure. The frequency of the oscillation also depended on the magnetic field. This is shown in Fig. 10. The vertical strokes mark the region in which the frequencies shifted with a fixed magnetic field, but whith varying pressure /41/. The lowest frequencies measured for each magnetic field depend linearly on the magnetic field and are above the cyclotron frequency in each case /42/. The measured frequencies are thus subject to the conditions applying in regions B and C of the dispersion diagram. Hence it can be assumed that the frequencies can be represented by the following relation:

$$f = k_1 \sqrt{f_c^2 + f_p^2}$$

where f_c = cyclotron frequency of the electrons, f_p = plasma frequency of the electrons. The term k_1 is a quantity depending on the parameters of the system. It is now assumed that the radius of the waveguide used as a basis for the calculation is equal to that of the beam for the parameters of Fig. 10. It then follows from the calculations in part B that k_1 is a quantity in the vicinity of 1 and does not vary much in the parameter range selected. On the other hand, it follows from the linear dependence of f on f_c that

$$f = C f_c$$

where C is a constant with $C > 1$. From these two equations for the frequency it then follows that

$$\frac{C}{k_1} = \sqrt{1 + \frac{f_p^2}{f_c^2}} = \text{const.} \qquad (28)$$

The result of this is that the oscillations begin when the ratio f_p/f_c exceeds a critical value depending on the parameters of the system. From Fig. 10 it follows that $C = 1.058$.

Assuming for k_1 the maximum value ($k_1 = 1$), one obtains from equation 28: $0.12 = f_p^2/f_c^2$ or $f_p = 0.35\, f_c$. This equation states that for the parameters of Fig. 10 the beam-plasma system is definitely stable if the condition

$$f_p \leq 0{,}35\, f_c$$

is satisfied. Since the dependence of the frequency on the magnetic field is about equal for other parameters, it can be stated in somewhat more general terms that the beam-plasma system is stable within wide limits if the condition

$$f_p < \sqrt{C^2+1}\cdot f_c$$

is satisfied. It has to be assumed that the oscillations always occur when the growth rate attains a certain value ω_i which can just compensate the damping; on the other hand, however, the oscillation occurs for a fixed ratio of f_p to f_c. It follows from this that the growth rate of the instability does not depend on f_p and f_c separately, but only on the ratio f_p/f_c. This, however, is the very behaviour that was found for the growth rate in the Doppler effect in region C.

The dependence of the smallest frequency on the magnetic field thus suggests that in the parameter range investigated there is interaction of the cyclotron wave in the beam with the cyclotron wave in the plasma and this leads to instability as the pressure continues to increase.

All these remarks are valid in the vicinity of the standard values: $I_B = 50$ mA; $U_B = 4$ kV; $B = 350$ gauss; $L = 40$ cm; beam radius $r = 2$ mm. If these values are further deviated from, the oscillations with the upper hybrid frequency are accompanied by others with larger amplitude. For magnetic fields above 550 gauss or small accelerating voltages below 3 keV, for example, sporadic oscillations with a frequency between about 100 and 350 Mc/s predominate. These oscillations constitute behaviour of the kind described by /42, 43/. The time-dependent behaviour of these oscillations was investigated on a fast oscilloscope. It could be seen that the oscillations begin, grow approximately exponentially, attain a maximum and then either decay immediately after - probably exponentially - or else remain at the maximum height for an indeterminate time. Various wave packets behaving in this way are not correlated with one another.

The upper hybrid frequency still occurs above 550 gauss as well and the stability condition also continues to be valid in this region. The stability criterion thus seems to have much more general significance than the assertion that the unstable state is caused by an instability in the region C.

The constant C determines the region of density n_o for which the system is definitely stable. C increases if the length is shortened or the current reduced. With otherwise equal parameters (standard values) a beam current of only 10 mA or a length of 13 cm gives $C \approx 1.15$. In the current range from 20 to 90 mA and for lengths between 20 and 50 cm there are only minor variations of C. Only when the currents are smaller and the lengths shorter, does C rise more steeply.

As can be seen from Fig. 10, a constant C_1 can be obtained from the maximum stable frequency attained and with this an instability criterion can be formulated: the system will definitely be in the turbulent state II if

$$f_p > \sqrt{\frac{C_1^2}{k_2^2}-1}\cdot f_c$$

Under the foregoing conditions k_2 is in this case a quantitiy for which $k_2 \lesssim 1$ is true. C_1 is also a constant which has the value 1.14 for standard parameters. C_1 has the same dependence on L and I_B as C. A stable plasma with $f_p > f_c$ seems to be obtained only for small beam currents and very short lengths.

V) Energy losses of the beam particles

a) Instability and spectrum of oscillations

This chapter deals with the phenomena of the turbulent system or state II. The most important aspect of this state are the high-energy losses of the beam particles. Before these are discussed in greater detail, however, the behaviour of the plasma column and a characteristic oscillation spectrum are described briefly.

The appearance of the plasma in the turbulent state varies as the pressure. High pressures (2×10^{-3} torr) cause a highly luminous plasma column whose diameter does not deviate much from that of the beam. With decreasing pressure in the region of about 5 to 4×10^{-4} torr there is a discontinuous change in appearance. The diameter of the luminous column becomes larger, its boundaries diffuse. With further decrease in pressure the diameter increases even more, at about 2 to 3×10^{-4} torr the plasma column becomes unsteady. In the vicinity of the critical pressure and below, the plasma column keeps still and the brighter luminosity fills a cylinder about 8 to 10 mm in diameter at 350 gauss. The change to the nonturbulent state on decrease of the pressure is just as sudden as the change to the unstable state on increase of the pressure.

Not much is known so far about the type of interaction and the oscillations in the turbulent region. It can be assumed /44/ that the turbulent state represents a turbulent plasma with oscillations that are coherent in some regions.
Fig. 11 shows an oscillation spectrum of the turbulent state for standard values just above the critical pressure. The frequency ranges from 0 to 2 Gc/s. The oscillations are spread over two frequency ranges: below 1 Gc/s and around 1.6 Gc/s. The cyclotron frequency is 980 Mc/s. Having made a study of the case $\omega_p > \omega_c$ analogous to that in Chapter A, one would expect oscillations below ω_c and below the upper hybrid frequency. If 1.6 Gc/s is assumed to be a frequency in the vicinity of the upper hybrid frequency, it follows that the plasma density has a minimum value

$$N_{e\,min} = 2 \times 10^{10} \; [cm^{-3}]$$

This value is an order of magnitude higher than that prior to the onset of instability. Outside the beam the density measured with probes also rises by about an order of magnitude after the onset of instability (Fig. 18). This then is some evidence that the high frequency peak is connected with the upper hybrid resonance.

The energy necessary for increasing the density can only be obtained from the beam energy. With the onset of instability the energy of the beam electrons has to undergo a change. On interaction of the beam with the plasma, part of the beam energy is used for exciting waves, heating the secondary (= plasma) electrons and thus finally for forming denser plasma.
Measurements of energy losses of the beam on interaction with a plasma without magnetic field are described in detail by URAMOTO /46/; other individual measurements without magnetic field in another parameter range are contained in / 48, 49, 50/. A few systematic measurements with magnetic field are described in / 31, 51, 52, 23, 53/. The present section makes a detailed and systematic investigation of the energy losses of the beam on interaction. The following section then discusses a few experiments for determining the energy absorption of the plasma.

b) General remarks on the measuring method

The energy losses of the electron beam were measured by means of a retarding field analyser. This is used to determine the current of the particles capable of overcoming a retarding voltage U_G. A few typical retarding field curves for various pressures can be seen in Fig. 12 /52/. The ordinate is the ratio of the target current at the retarding voltage U_G to the current at the retarding voltage $U_G = 0$, while the retarding voltage U_G is taken as the abscissa. At 1.5×10^{-5} torr there is as yet no interaction, the beam energy being practically monochromatic. At 1.5×10^{-4} torr, on the other hand, the discharge is turbulent, the particle energies being scattered from 0 to above the accelerating voltage ($U_B = 4$ keV). At 2×10^{-3} torr as well there is still considerable interaction, and here, too, particles are still accelerated beyond the initial energy. The slope of the curves is as in the case of thermal motion with superposed drift (Fig. 17). On closer inspection it can be seen, however, that no thermal motion is really involved because the decrease of the distribution function to high-energy electrons takes place too fast.

The area below the curves represents the energy transmitted per second to the target. The difference between the areas with and without turbulence gives the energy expended per sec by the beam in exciting and amplifying waves. In most cases the area below the curves can be approximated by a trapezium. This is replaced by a rectangle of equal area. In this way a new average energy eU_a of the particles is defined. The difference between eU_B and eU_a:

$$\Delta eU = \Delta E = eU_B - eU_a$$

gives the average energy lost by one particle on passing through the plasma. It is this value ΔE which will be discussed in the following.

The vertical strokes on the curves (Figs. 13 to 16) give the arithmetic mean of the measuring error. This error is composed of the reading error and the actual scattering of the energy losses. The maximum energy losses as a function of the pressure were determined for a fixed set of parameters by measuring the energy loss curve in the vicinity of the supposed maximum at about 6 different pressures. The maximum loss was then found from these six curves. This operation was repeated in succession and at various times, five times mostly. In this way about five experimental values scattered about a mean value are obtained for one set of parameters. The arithmetic mean of these five values and that of the measuring error were plotted.

c) Results of the measurements

Figs. 13 to 16 show the measuring results. The mean energy loss of a particle after passing through the plasma is plotted in each curve.

First the energy loss is shown in Fig. 13 as a function of the pressure. Not counting the boundary values, it is possible in the large to ascertain two different levels for the energy losses: a higher level of 1 keV or approx. 25 % of the initial energy in the region of 2 to 4×10^{-4} torr and a lower level of 0.65 keV or approx. 15 % of the initial energy in the pressure range from 6×10^{-4} to 10^{-3} torr. The gradient at 5×10^{-4} torr coincides with the visible change of the plasma column described at the beginning of this chapter. Above 10^{-3} torr the plasma column is sharply defined. The energy losses decrease continuously with increasing pressure.

The losses cannot be explained, of course, by excitation and ionization of neutral gas because the losses would then have to rise with the pressure. The losses due to binary collisions are very small. For ionization at 10^{-2} torr they have the small value 0.015 keV.

In the vicinity of 2×10^{-4} torr there is some uncertainty in the measurement. This is approximately the region in which the plasma column begins to sway unsteadily. The number of fast and slow particles with respect to the intermediate particles seems to be too severely

reduced compared with the slope of the curves at other pressures. With even lower pressure and a steady plasma column the distribution function takes the form shown in Fig. 12. The energy losses attain a maximum.

Below the pressure for the last experimental value the energy losses probably increase still more. They then depend, however, to a great extent on the number of electrons reflected in the retarding field. The distribution function (and the appearance of the plasma column as well) therefore varies with the retarding voltage. It is then no longer possible to measure nor is there any point in it any more.

The dependence of the maximum loss and the loss at a fixed pressure of 10^{-3} torr on the accelerating voltage is given in Fig. 14. The absolute energy losses increase with the accelerating voltage, i.e. with the initial energy. The relative losses, on the other hand, have a higher value at low voltages. At accelerating voltages of 1.5 kV the losses attain values of nearly 50 % of the initial energy. At 10^{-3} torr the losses are smaller but have about the same dependence on the voltage as the maximum losses.

The dependence of the energy losses on the length of the system is shown in Fig. 15. If the system is shortened from a length of 40 cm to about 17 cm, the maximum energy losses do not vary much. There is no appreciable reduction of the losses until the length is shortened more. The neutral gas pressure for the maximum losses with lengths $L > 17.5$ cm is in the region below 6×10^{-4} torr, i.e. in the range which occupies the upper level in Fig. 13. With shorter lengths the neutral gas pressure required for attaining the maximum loss increases sharply. The energy losses lie in the region of the lower level and below.

The last series of measurements (Fig. 16) shows the dependence of the energy losses on the distance from the beam centre. The energy losses reach a maximum at the boundary of the beam. The measuring error was estimated in Fig. 16 at 10 %. It was not possible in this case to form mean values because the zeros of the scale for the radius were different each time. A point of maximum beam density was chosen as zero. This, however, should not necessarily be equated with the centre of the beam (see Chapter C III). All measurements in Figs. 13 to 15 were made at a point of maximum beam density.

It is surprising that the energy loss curve has a maximum at the boundary of the beam. The beam density is about an order of magnitude smaller at the point of the maximum than in the centre. If it is assumed that roughly the same model applies in state II as in state I, one would expect higher fields for higher beam densities, particularly at the boundary of the beam for the electric field strength in the direction of the magnetic field
It then follows that there should be also an energy loss $\Delta E = 0$ at the edge of the beam. The maximum of the energy loss at the boundary therefore shows that we are not justified in taking a waveguide with the diameter of the beam as a model of the system in the unstable state. For wave propagation one probably requires a waveguide with a much larger diameter - perhaps that of a highly luminous column, which has a constant plasma density according to Fig. 20.
The energy distribution functions for the maximum at the edge of the beam have only a very small proportion of fast electrons. The lack of fast electrons does not account for the increase of the losses (these being greater than the reduction of the gains) but it is extremely conspicuous.

d) Possible explanations of the loss curves

The energy losses occurring on the interaction of an electron beam with a plasma are so vitally important , their dependence on the parameters of the system so pronounced that they clamour for a theoretical interpretation. No general, detailed theory exists as yet, un-

fortunately, nor is there any clear-cut idea of the non-linear phenomenon of interaction.

The works of SHAPIRO and FAINBERG /53,54/ are the most detailed available and those most in line with the experiment described here. The authors make a non-linear, but one-dimensional calculation without magnetic field (only plasma frequencies are involved in an interaction) of the interaction of an electron beam with a plasma. The theories are only valid if the condition

$$n_o T_o \gg n_o' m v_o'^2$$

is satisfied, T_o being the temperature of the plasma electrons in eV.
This condition means that the oscillation energy determined by the energy in the beam has to be small compared with the thermal energy of the plasma electrons. Otherwise, the theory would have to allow for the reaction of the oscillations on the plasma density and temperature.

This condition is just satisfied for plasma densities $n_o \approx 10^{11}$ cm^{-3}, plasma temperatures of 10 eV, beam densities of 10^8 cm^{-3} and beam energies of 4 keV. In /5 / it is reported that for $n_o T_o \approx n_o' m v_o'^2$ the calculation still gives the correct result, at least as regards the order of magnitude. Since no other theories are available, the experimental results here should be compared with those of the works quoted.

The authors assume that the excited oscillations cause the beam electrons to diffuse in the velocity space, the direction of diffusion being such that the two-group distribution function changes into a plateau extending from the velocity of the beam electrons to that of the plasma electrons. On this assumption they calculate the spectrum of oscillations pertaining to this final state. In addition, they calculate the electric energy and the potential energy in the oscillations, the variation in temperature and density of the plasma and the variation in temperature and mean velocity of the beam electrons. Here it is the last two quantities that are primarily of interest.

The thermal energy of the beam electrons in the final state is given by

$$\frac{n'T'}{2} \approx \frac{1}{12} \frac{n' m v_o'^2}{2}$$

That is, the thermal energy in the beam is about a twelfth of the initial beam energy.

For the variation of the mean energy of the beam electrons they find

$$\Delta\varepsilon = \frac{3}{4} \frac{n' m v_c'^2}{2}$$

From these two equations it follows that 1/12 of the translation energy of the beam is converted into thermal energy of the beam and 2/3 into radiant energy. That is, the total energy loss of the beam could be a maximum of 66 %.
For the standard value of 4 keV of our experiment the above formulae give for the thermal energy

$$T' \approx 0.33 \text{ keV}$$

and for the mean drift velocity

$$eU_o \approx 1 \text{ keV}$$

The integral current distribution function is calculated as a function of the voltage for a Maxwell distribution of the beam electrons with superposed drift for various ratios W of drift energy eU_D to thermal energy T (see Appendix B). This gives Fig. 17. Comparison of the calculated and measured curves shows that the curve W = 3 is most like the measured curve at 1.5×10^{-4} torr (compare Fig. 12). This ratio is in fact exactly equivalent to the W calculated by SHAPIRO, but a more accurate comparison shows that the drift velocity cannot be 1/4 of the original beam velocity, as required. The original voltage U_B for W = 3 is in

fact about 0.37 $(\sqrt{5} + \sqrt{W^*})^2$. This value corresponds to 4 keV/T. This gives a temperature of 0.69 keV and a drift energy of almost 2.1 keV. The energy loss comes to 1.21 keV or 30% of the initial energy. The values for temperature and drift are twice as high as those calculated, while the total energy loss is only half as high. Nevertheless, the calculation correctly reproduces the experimental results with respect to the order of magnitude. In the theory, collision damping and the temperature of the electrons, which lead to a reduction of the maximum attainable fields and hence to smaller energy losses, are not taken into account; furthermore, the model on which the theory is based does not exactly reproduce the experimental conditions. +In general, however, it can be concluded from the comparison that the interaction on which the experiment is based is almost of the same intensity as the interaction postulated in the calculation. In /54/ FAINBERG and SHAPIRO calculate the structure of the excited wave fields. They find that the oscillation energy - and hence the region of the energy loss - is concentrated in two layers close to the region where the beam enters the plasma. These layers should extend for only a few wavelengths - a few cm in our case. It is thus obvious that the energy losses practically do not depend on the length.

The energy loss calculated in /53,54/ is independent of the beam current and beam velocity. This is confirmed by the measuring results insofar as no dependence of the maximum energy loss on the beam current could be ascertained in the experiment. The results, however, are not independent of the beam velocity.

From /53,54/ we learn nothing of the dependence on the radius because a one-dimensional model is used in these investigations. The increase of the energy losses towards the boundary points to a concentration of the fields at the boundary.

The minimum strength of the fields can be estimated from the maximum energy loss. With a length of about 15 cm there are still electrons which have lost all their energy of, for example, 4 keV. From this an electric field strength of 266 V/cm in the direction of the beam can be calculated. This field is minimum, if it is born in mind that the main fields are probably concentrated in a much smaller region and if it is assumed over and above that the maximum loss is 4 keV. The "loss" can, however, be greater in actual fact. As the comparison of the calculated distribution function with the experiment demonstrates, this is because not only can electrons in the wave fields be slowed down, they can even be accelerated backwards as well.

VI) Properties of the plasma surrounding the beam

Having considered the energy losses of the beam, let us now deal briefly with the energy gains of the plasma. The term "plasma" is used here to refer to the plasma surrounding the beam. The conditions in the plasma were measured with plane Langmuir probes whose surface normal is directed parallel to the magnetic field. The probe was 3 mm in diameter. It was possible to evaluate the probe curves from both the ion current and the electron current. The qualitative agreement of the results was good; quantitatively they were at least of the same order of magnitude. Hydrogen was used as working gas for the density and temperature measurements.

First the plasma density and the temperature in the vicinity of the beam were measured as a function of the pressure. The results are given in Fig. 18. Here the density, electron saturation current and temperature are plotted. In the stable region the electron saturation current and the density increase approximately in proportion to the square of the neutral gas pressure. At even lower pressures the rise often tends to be linear. Just below the critical pressure the plasma density again drops, reaches a minimum and at the critical pressure jumps to a value about 1+1/2 orders of magnitude greater /35/. As the pressure in-

---

+Under favourable conditions (Fig.14, at 1.5 kV) we also obtained energy losses of almost 50 %.

creases further the density reaches a maximum and then drops at higher pressures. The measuring error for the individual experimental points may be very high /35/. After a large number of these curves have been evaluated for various arc currents, voltages and magnetic fields, it can, however, be stated that the minimum in the density below the critical pressure is not due to measuring errors. The density range in which the density drop takes place is the very region in which the oscillations causing the turbulence occur. The drop in density is accompanied by a rise in temperature. Even if one has to assume that the experimental points of the temperature involve a substantial error of many percent the thermal distribution may still be regarded as reproducible. This can also be deduced from the evaluation of many other curves. The two temperatures T_1 and T_2 represent two different groups of electrons: a slow, dense group with the temperature T_1 and a fast group with the temperature T_2. Even if the two temperatures are regarded only as the upper and lower margin of error, it follows from the thermal distribution that the temperature of the electrons rises approximately when the oscillations begin; after attaining a maximum of about 9 eV at a pressure just above the critical pressure, the temperature then drops again to values of 1 eV at pressures of 10^{-3} torr.
The drop in density with increasing pressure in the stable region is due, firstly, to the decrease in the energy losses of the beam and, secondly, to the contraction of the plasma. The probe, which is at a fixed distance from the beam, hereby passes in turn through various density ranges of the plasma.
The maximum measured density of 2×10^{10} cm^{-3} agrees with the density calculated from the oscillation spectrum of the turbulent state on the assumption that the maximum amplitude at 1.65 Gc/s corresponds roughly to the upper hybrid frequency. For this measurement the probe was located in the highly luminous plasma column, whose density is almost constant. This is shown in Fig. 20.
The dependence of the density, electron saturation current and temperature was measured as a function of the distance of the probe surface from the boundary of the beam in the nonturbulent and turbulent state. In the nonturbulent state (Fig. 19) the density decreases sharply from the boundary onwards. The temperature also drops towards the outside. The maximum temperature measured at the beam boundary did not exceed about 3.2 eV.

With turbulence the situation is different (Fig. 20). The density is constant in the vicinity of the beam to a distance of almost 1 cm, and only then does it drop almost exponentially. The temperature now attains values of almost 8 eV at the beam boundary, but then drops quickly outwards, decreasing to values of about 1 eV at some distance from the beam.
The largest jump in density occurs about 1 cm from the beam. This jump is more than two orders of magnitude. For high magnetic fields (approx. 1100 gauss) this distance from the boundary of the beam could be taken roughly as the boundary of the intense luminosity.

VII) Further observations of the system

a) Influence of secondary electrons from the collector

The influence of secondary electrons on ion oscillations in the low pressure range is described by AGDUR /55/. His conclusion is that reflected electrons are not necessary for exciting ion oscillations. Our investigation is concerned with whether and to what extent secondary electrons are necessary for exciting the plasma instability.
The term "plasma instability" is again used here to refer to the occurence of intense luminosity or increased energy loss, not to the occurrence of oscillations in particular.

The entry diaphragm into the retarding field was enlarged to the size of the beam diameter. The retarding voltage U_G was then varied in the region of the accelerating voltage U_B. If U_G was a little higher than U_B all beam electrons were reflected in the nonturbulent state. If U_G was smaller than U_B all electrons reached the collector. Unfortunately, the number of measurements with this system was restricted. This was because, for one thing, the collector was not constructed for absorbing high energies. Another reason was that so many particles were reflected in the turbulent case and then accelerated again that they impinged once more on the hot cathode and destroyed it. For standard values the few measurements showed that with reflection only about half the critical pressure was necessary to cause instability. The system also became unstable and turbulent, however, without reflected electrons.
For small beam currents or short length the influence of the reflected electrons is more difficult to estimate. Measurements of the energy loss have shown here that at critical levels the system is only unstable, i.e. shows high energy loss, if the full retarding voltage is applied. If the retarding voltage in the analyser drops, the intense luminosity often persists in a milder form, but there are no longer slow particles in the energy distribution of the electrons investigated. The "instability" then no longer exists, at least not in the column above the analyser diaphragm.
The turbulent state accompanied by energy loss of the investigated particles can also be restored without retarding voltage by raising the pressure.

b) Beam plasma with externally excited frequencies

For a time the experiments were conducted in a slotted Cu tube with an internal diameter of 26 mm. The essential phenomena remained the same, only the critical pressures increased. A probe for measuring the oscillations along the column passed through one of the two slots in the metal tube. A fixed probe projected approximately into the centre of the vessel through the other slot. Applying the latter probe to a RF signal generator produced a plasma in the metal tube for $\omega = \omega_c$. The original intention of this experiment, which was to excite the oscillations produced in the beam-plasma system with a pin probe, was unsuccessful. Even when the plasma oscillations were present there was no resonance.

When, on the other hand, the oscillations were present and the probe produced a plasma for $\omega = \omega_c$, the amplitude and the frequency of the oscillations increased. This effect was exactly the same as that obtained by raising the pressure. The frequencies thus do not couple. Only after the plasma density increases do the beam-plasma oscillations change. (The situation is different in an experiment of ETIEVANT: if the signal generator is connected to a helix around the beam, there is resonance at the upper hybrid frequency /56/.)

c) Low-frequency oscillations in the unstable state

The RF oscillation spectrum in the turbulent state was described in C Va. Broad-band oscillations, as yet unidentified, were also found in the low-frequency range. Their frequency was in the region of a few 100 kc/s. It was often possible to find six harmonics of the fundamental frequency. The frequency of the oscillations drops as the magnetic field rises to about 1100 gauss and then remains constant up to about 1500 gauss. The frequency also drops with the pressure. The frequency of the oscillations

does not depend on the radius. There is also a drop in frequency with increasing beam velocity and decreasing beam current (constant output).

d) Fast electrons and X-rays

As was first reported by ALEXEFF and NEIDEIGH /34/ and then also by BEREZIN et. al. /51/, fast electrons are produced on interaction of an electron beam with a plasma. In our experiment the energies of the particles ranged up to a maximum of 5 keV for standard values. A total of about 15 to 20 % of the beam electrons had gained energy. The maximum gain of a particle, however, amounts at most to 25 % of its original energy. When the experiment conformed to the described set-up there were no X-rays. Otherwise, this would have indicated a very high particle energy.

When, however, the magnetic field was varied so that the homogeneous field was made into a mirror field, X-rays were detected outside the glass container with high magnetic fields (1000 - 2000 gauss) and the smallest possible pressures in the unstable range. This radiation did not come from the plasma volume or the walls, but almost exclusively from the target. The intensity of the radiation was reduced by about half by being passed through a 15 mm thick sheet of aluminium. From this the mean energy is estimated at between 50 and 80 keV. At a distance of 10 cm from the target and through a 6 mm thick glass wall the intensity of the radiation attains values of up to 60 mr/h. Since the apparatus was not suitable for high stationary magnetic fields, this type of experiment was not pursued.

Acknowledgements

Dr. v. Gierke, who suggested this experiment, is hereby thanked for his constant support. I am also grateful to Professor E. Fünfer for the opportunity of submitting this work as a thesis.
Appreciation is due as well to my colleague, Mr. A. Borer, for numerous discussions and suggestions.
Finally, I should like to acknowledge the work of Miss H. Müller, who programmed the calculations, to Mr. Weber for assistance in the experiments and Mr. Nicol for translation of this report into English language.

Appendix A

Calculation of a simple diffusion model

Fig. 21 gives measurements of the floating potential as a function of the distance from the beam. The curves show that the potential at the edge of the beam is negative in the pressure range without turbulence. At a distance of about 1 cm from the beam the potential becomes positive.

Without turbulence there is a marked surplus of electrons in the beam and a surplus of ions outside. The plasma outside the beam is positive because the electrons parallel to the magnetic field diffuse faster than the ions. Thus outside the beam the diffusion of the charged particles is determined by the velocity of the ions. Because of the space charge of the beam electrons the charge in the beam is negative, at low pressures at least. At higher pressures the electrons of the secondary plasma are quickly lost to the end plates and the slow ions compensate the space charge. This continues until the space charge drops to, for example, the value -U. This value is such that a few ions can already leave the beam radially because of their thermal energy and their large Larmor radii. At the same time less secondary electrons flow away to the ends because of the reduced potential. The value -U now becomes such as to bring about equilibrium between these two processes.

Along the outside of the beam the floating potential is constant - as was measured - and only in a very small region near the ends is there a jump. The plasma outside the beam is thus without electric fields in z-direction on the whole. The same can also be assumed with a high degree of probability for the plasma in the region of the beam.

Under these conditions it is now possible to comment on the density of the plasma outside the beam. Its value is such that there is equilibrium between productive and destructive processes. The productive process probably consists mainly of the radial diffusion of ions from the beam into the surrounding plasma. All that is important here, however, is that the productive processes along the beam can be assumed to be constant. The diffusion parallel to the magnetic field is regarded as the predominant loss process. In the given situation it is determined by the velocity of the ions. For the region outside the beam we thus obtain the equation

$$- D_{i\parallel} \frac{d^2 n}{dz^2} = N_+$$

where N_+ is the production rate and $D_{i\parallel}$ the diffusion coefficient of the ions. If the density at the ends of the system is assumed to be zero, it follows that

$$n(z) = \frac{N_+ \cdot z}{2 D_{i\parallel}} (L - z) \tag{29}$$

The density maximum n_o is given for $z = L/2$ and is calculated as

$$n_c = \frac{N_+ L^2}{8 D_{i\parallel}} \tag{30}$$

The density in the centre of the system is proportional to the square of the length.

In one experiment a probe was placed at a fixed distance L_o from one end of the plasma column. The other end of the plasma column was movable. Eq. (29) then gives the following dependence of the density on the difference of the lengths $L - L_o = \Delta L$:

$$n(L_c) = \frac{N_+ L_c}{2 D_{i\parallel}} (L - L_o) = K \cdot \Delta L$$

The experiment, however, gives the following result

$$n(L_0) = k'(\Delta L + L_x)$$

The length L_x takes into account the influence of the sheath at the end of the plasma. This sheath acts like a plasma column with the length L_x. Instead of (30) the maximum length then becomes

$$n_c = \frac{N + (L + 2L_x)^2}{8 D_{in}} \tag{30a}$$

The plasma in the region of the beam can be treated in the same way, if allowance is made for the fact that the diffusion is here determined in accordance with the model by the velocity of the electrons. Furthermore, the production process is due to the ionization of the beam electrons. We then obtain for the density the same form as in (30a). We now take into account the fact that the production rate is proportional to the beam current and the pressure, but that the diffusion constant is inversely proportional to the pressure. The maximum plasma density obtained in the beam is

$$n_c = C \cdot I \cdot p^2 (L + 2L_y)^2 \tag{31}$$

L_y is the length, corresponding to the influence of the sheath.
The plasma density in the beam is proportional to the beam current, to the square of the pressure and to the square of the length.

Appendix B

Calculation of the integral energy distribution of the beam electrons from the drift and temperature.

A Maxwell distribution with superposed drift is written

$$f(v) = \frac{m}{(2\pi m k\bar{T})^{1/2}} \exp\left(-\frac{m}{2k\bar{T}}(v - v_0)^2\right)$$

For the measurement with retarding field only the distribution in the z-direction is of interest. The current to the target is composed of the particles with a velocity between 0 and ∞ :

$$j_0 = e n_0 \int_0^\infty v f(v)\, dv \tag{32}$$

j has to be found as a function of the voltage:

$$v = \sqrt{\frac{2eV}{m}} \qquad v_D = \sqrt{\frac{2eV_D}{m}}$$

With $\frac{eV}{kT} = U$; $\frac{eV_D}{kT} = W$, (32) is written after a short calculation

$$j_0 = e n_0 \left(\frac{k\bar{T}}{2\pi m}\right)^{1/2} \int_0^\infty \exp\left[-\left(\sqrt{V} - \sqrt{W}\right)^2\right] dV$$

We want to find the current of the particles which can exceed a certain potential E_1:

$$j(E_1) = e n_0 \left(\frac{k\bar{T}}{2\pi m}\right)^{1/2} \int_{E_1}^\infty \exp\left[\left(\sqrt{V} - \sqrt{W}\right)^2\right] dV$$

This equation was numerically calculated for various ratios W. Fig. 17 shows $\frac{j(E_1)}{e n_0 \left(\frac{k\bar{T}}{2\pi m}\right)^{1/2}}$ as a function of E_1.

LITERATURE REFERENCES

/1/	W.O. Schumann	Z.f.Physik, 121, 17, (1943)
/2/	J.R. Pierce	J.Appl.Phys.19, 231, (1948)
/3/	D. Bohm, E.P. Gross	Phys.Rev. 75,1851, (1949) Phys.Rev. 75,1864, (1949) Phys.Rev. 79, 992, (1950)
/4/	A.I. Achiezer, Ya.B. Fainberg	Zh ETF 11, 262, (1951)
/5/	K.N. Stepanov, A.B. Kitsenko	Sov.Phys.- Techn.Phys. 6, 120, (1961)
/6/	A.J. Lichtenberg, J.S. Jayson	J.Appl.Phys.36, 449, (1965)
/7/	O.E.H. Rydbeck, H. Wilhelmsson	Proc. 4th Intern. Conf.on Ionization Phenomena in Gases, Uppsala 1959, S. 653
/8/	H.E. Singhaus	Phys.of Fluids 7, 1534, (1964)
/9/	R. Gerwin, D.J. Nelson	Boeing Report D1-82-0332 (1964)
/10/	B.N.A. Lamborn	Phys.Fluids 7, 292, (1964)
/11/	E.G. Harris	Phys.Fluids 7, 1572, (1964)
/12/	V.F. Kuleshov, A.A. Rukhadze	Sov.Phys.-Techn.Phys. 9, 449, (1964)
/13/	M.F. Gorbatenko	Sov.Phys.-Techn.Phys. 8, 123, (1963)
/14/	M.F. Gorbatenko	Sov.Phys.-Techn.Phys. 8, 789, (1964)
/15/	A.J. Lichtenberg	AFCRL-63-195, Series No. 60, Issue No. 490
/16/	A.J. Lichtenberg	IEEE Trans.Elec.Devices, ED11, 62, (1964)
/17/	P.E. Serafim	Quarterly Progress Report of Res.Lab.Electronics, MIT, 15.1. (1962)
/18/	K.S. Karplyuk, S.M. Levitskii	Sov.Phys.-Techn.Phys. 9, 1063, (1965)
/19/	B.J. Maxum, A.W. Trivelpiece	J.Appl.Phys. 36, 481, (1965)
/20/	M.T. Vlaardingerbroek, K.R.U. Weimer	H.J.C.A.Nunnink Phil.Res.Rep. 17, 344, (1962)
/21/	A.W. Trivelpiece, R.W. Gould	J.Appl.Phys. 30, 1784, (1959)
/22/	C. Etievant	Rapport CEA-R 2456
/23/	V. Bevc, T.E. Everhart	J.Electr.Contr.13, 185, (1962)
/24/	J.E. Scharer, A.W. Trivelpiece	J.Appl.Phys. 36, 318, (1965)
/25/	B. Agdur, B. Enander	J.Appl.Phys. 33, 575, (1962)
/26/	L.D. Smullin, W.D. Getty	Phys.Rev.Letters 9, 3,(1962)
/27/	R.J. Briggs	Electron Stream Interaction with Plasma, Res.Monograph No.29 The MIT Press, Cambridge, Mass.
/28/	P.A. Sturrock	Phys.Rev. 112, 1488, (1958)
/29/	B. Vural	RCA Rev. 12, 753, (1961)
/30/	I.F. Kharchenko, Ya.B. Fainberg, et al.	Conf.on Plasma Physics and Controlled Nuclear Fusion Research, Salzburg, 1961, S. 1101
/31/	I.F. Kharchenko, Ya.B. Fainberg, et al.	Sov.Phys.-Techn.Phys. 6, 551, (1962)

/32/	L.D. Smullin, W.D. Getty	Phys.Rev.Letters 9, 3, (1962)
/33/	W.D. Getty, L.D. Smullin	J.Appl.Phys. 34, 342, (1963)
/34/	I. Alexeff, R.V. Neidigh, et al.	Phys.Rev. 136, A 689, (1964)
	I. Alexeff etc.	Phys.Rev.Letters 10, 273, (1963)
/35/	P. Hedvall	J.Appl.Phys. 33, 2426, (1962)
/36/	J.E. Hopson	J.Appl.Phys. 34, 2425, (1963)
/37/	I.F. Kharchenko, Ya.B. Fainberg, et al.	Sov.Phys.-Techn.Phys. 9, 798, (1964)
/38/	H.R. Johnson	Proc.of the IRE 43, 684, (1955)
/39/	D.A. Dunn, W. Nichparenko	J.Appl.Phys. 36, 3273, (1965)
/40/	W. Herrmann	Paper presented at the 7th Inter. Conf.on Phenomena in Ionized Gases, Belgrade 1965
/41/	R. Targ, L.P. Levine	J.Appl.Phys. 32, 731, (1965)
/42/	A. Vermeer, H.J. Hopman et al.	Paper presented at the 7th Inter. Conf. on Phenomena in Ionized Gases, Belgrade 1965
/43/	H.J. Hopman	Euratom Symposium on Plasma Physics Varenna 1964. Part II, Page 21
/44/	T.H. Stix	Phys.Fluids 7, S.1960, (1964)
/45/	J.R. Apel, A.M. Stone	Paper presented at the 7th Inter. Conf.on Phenomena in Ionized Gases, Belgrade 1965
/46/	J. Uramoto	IPPJ-22-1964
/47/	A.K. Berezin, Ya.B. Fainberg, et al.	Plasma Physics (J.Nucl.Energ. Part C) 4, 291, (1962)
/48/	I.F. Kharchenko et al.	Proc. 4th Inter.Conf. on Ionization Phenomena in Gases,Uppsala 1959,p.671
/49/	I.F. Kharchenko et al.	Sov.Phys.-JETP 11, 493, (1960)
/50/	A.R. Beresin, et al.	Sov.Atomic Energy 14, 245, (1963/64)
/51/	I.F. Kharchenko	J.Nucl.Energ. 6, 201; (1964)
/52/	M.V. Nezlin	Sov.Phys. JETP 19, 26, (1964)
/53/	V.D. Shapiro	Sov.Phys. JETP 17, 416, (1963)
/54/	Ya.B. Fainberg, V.D. Shapiro	Sov.Phys. JETP 20, 937, (1965)
/55/	B. Agdur	Ericsson Technics No.1, (1960
/56/	C. Etievant	Private communication
/57/	R. Kippenhahn, H.L. De Vries	Z.f. Naturforschung 15a, 506, (1960)
/58/	E. Canobbio, R. Croci	Z.f. Naturforschung 16a, 1313, (1961)
/59/	C. Etievant, R. der Agobian	Conf.on Plasma Physics and Controlled Nuclear Fusion Research, Salzburg, 1961, p. 1025
/60/	E. Canobbio, R. Croci	Proc. 5th Inter.Conf., Munich 1961, p. 1293
/61/	E. Canobbio	Nucl.Fusion 1, 172, (1961)

FIGURE CAPTIONS

Fig. 1 Dispersion diagram; frequency and growth rate as a function of wave number.

Fig. 2 Growth rates as a function of the reciprocal product of the radius r and magnetic field strength B with constant beam current I_B and constant plasma density ω_p.

Fig. 3a Growth rates as a function of the plasma density.
Fig. 3b Frequencies as a function of the plasma density.

Fig. 4 Frequencies and growth rates as a function of the radius and the various radial modes. $p_{o\nu}$ are the zeros of the Bessel function

Fig. 5 Frequencies as a function of the reciprocal product of the beam radius and magnetic field with constant beam current and constant plasma density.

Fig. 6a Schematic diagram of the apparatus.
Fig. 6b Magnetic field strength along the apparatus.

Fig. 7a Critical pressure as a function of the beam current.
Fig. 7b Critical pressure as a function of the accelerating voltage.

Fig. 8a Critical pressure as a function of the magnetic field.
Fig. 8b Critical pressure as a function of the interaction length.

Fig. 9 Beam density profile.

Fig. 10 Frequency ranges at various pressures as a function of the magnetic field.
Fig. 11 Oscillation amplitude as a logarithmic function of the frequency.

Fig. 12 Retarding field curves. Reduced target current as a function of the retarding voltage U_G at various pressures.

Fig. 13 Energy loss ΔE as a function of the pressure.

Fig. 14 Energy loss ΔE as a function of the accelerating voltage.

Fig. 15 Energy loss ΔE as a function of the beam length L.

Fig. 16 Energy loss ΔE as a function of the distance Δr from the beam centre.

Fig. 17 Calculated retarding field curves for various temperatures and drifts.

Fig. 18 Density probe current and temperature as a function of the pressure.

Fig. 19 Density probe current and temperature as a function of the radius in the nonturbulent state.

Fig. 21 Floating potential as a function of the distance from the beam.

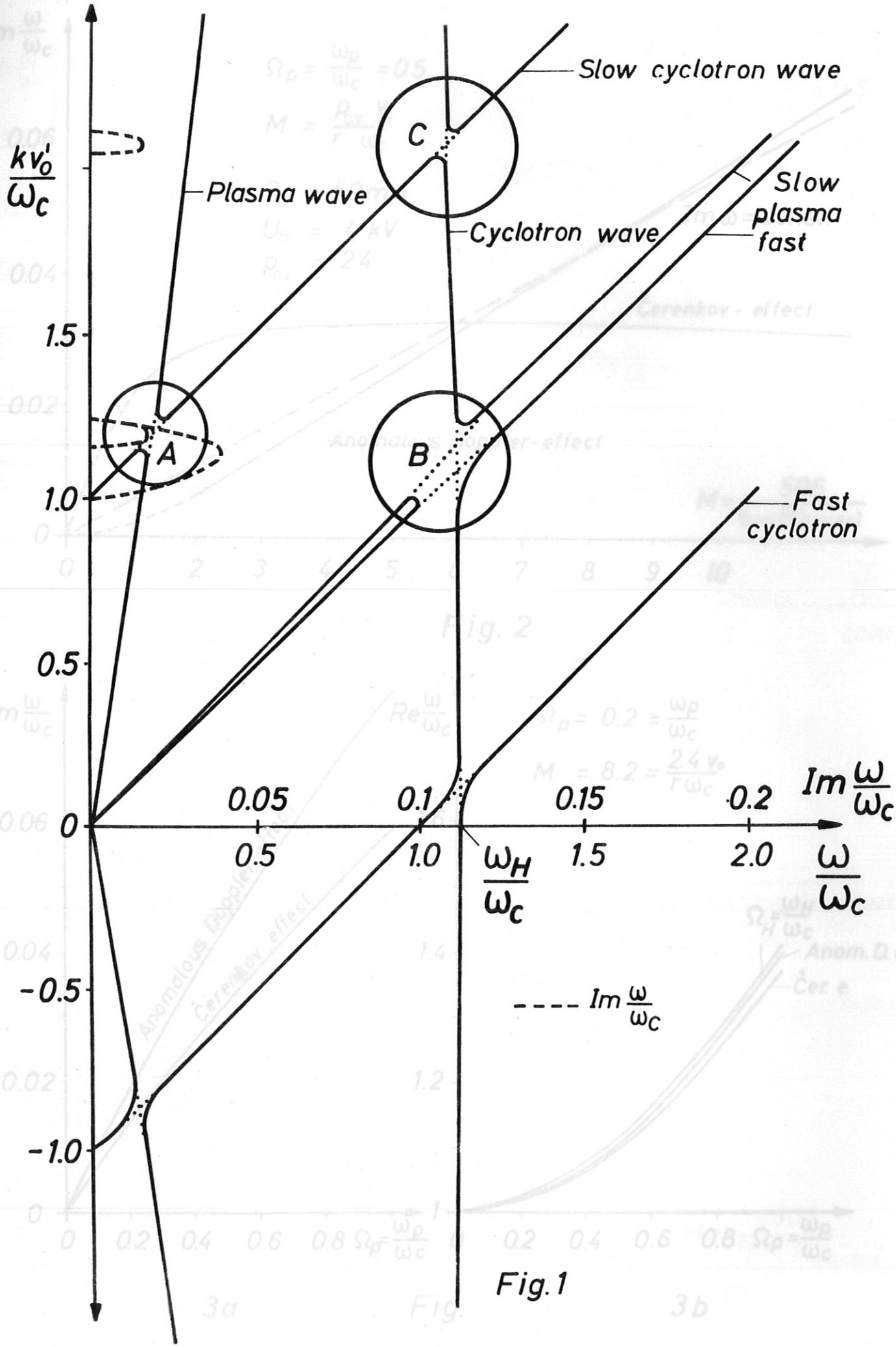
Slow cyclotron wave
Plasma wave
Cyclotron wave
Slow plasma fast
Fast cyclotron
A
B
C
$\frac{kv_0'}{\omega_c}$
1.5
1.0
0.5
0
-0.5
-1.0
0.05
0.1
0.15
0.2
$Im\frac{\omega}{\omega_c}$
0.5
1.0
$\frac{\omega_H}{\omega_c}$
1.5
2.0
$\frac{\omega}{\omega_c}$
---- $Im\frac{\omega}{\omega_c}$

Fig. 1

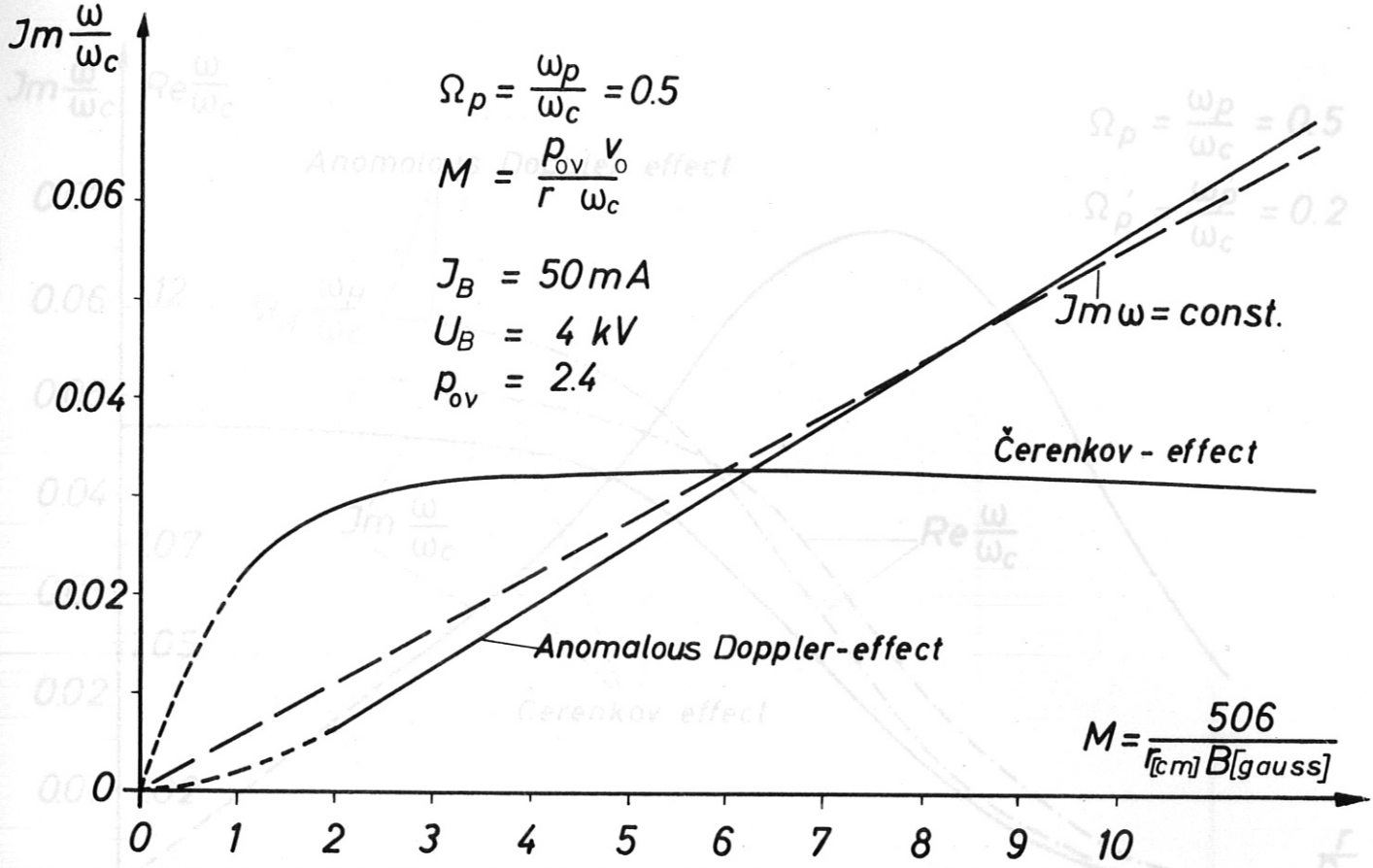

Fig. 2

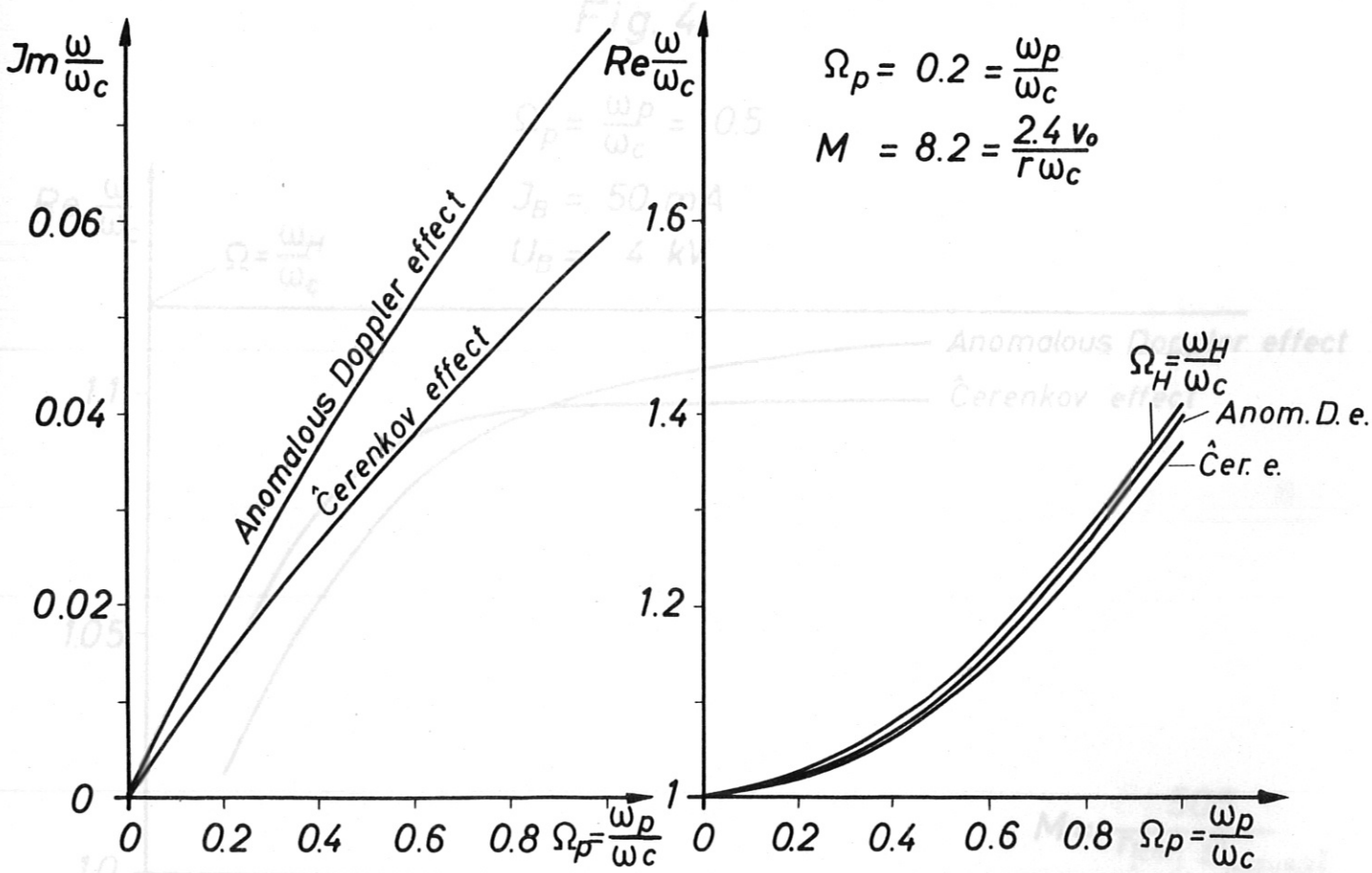

3a Fig. 3b

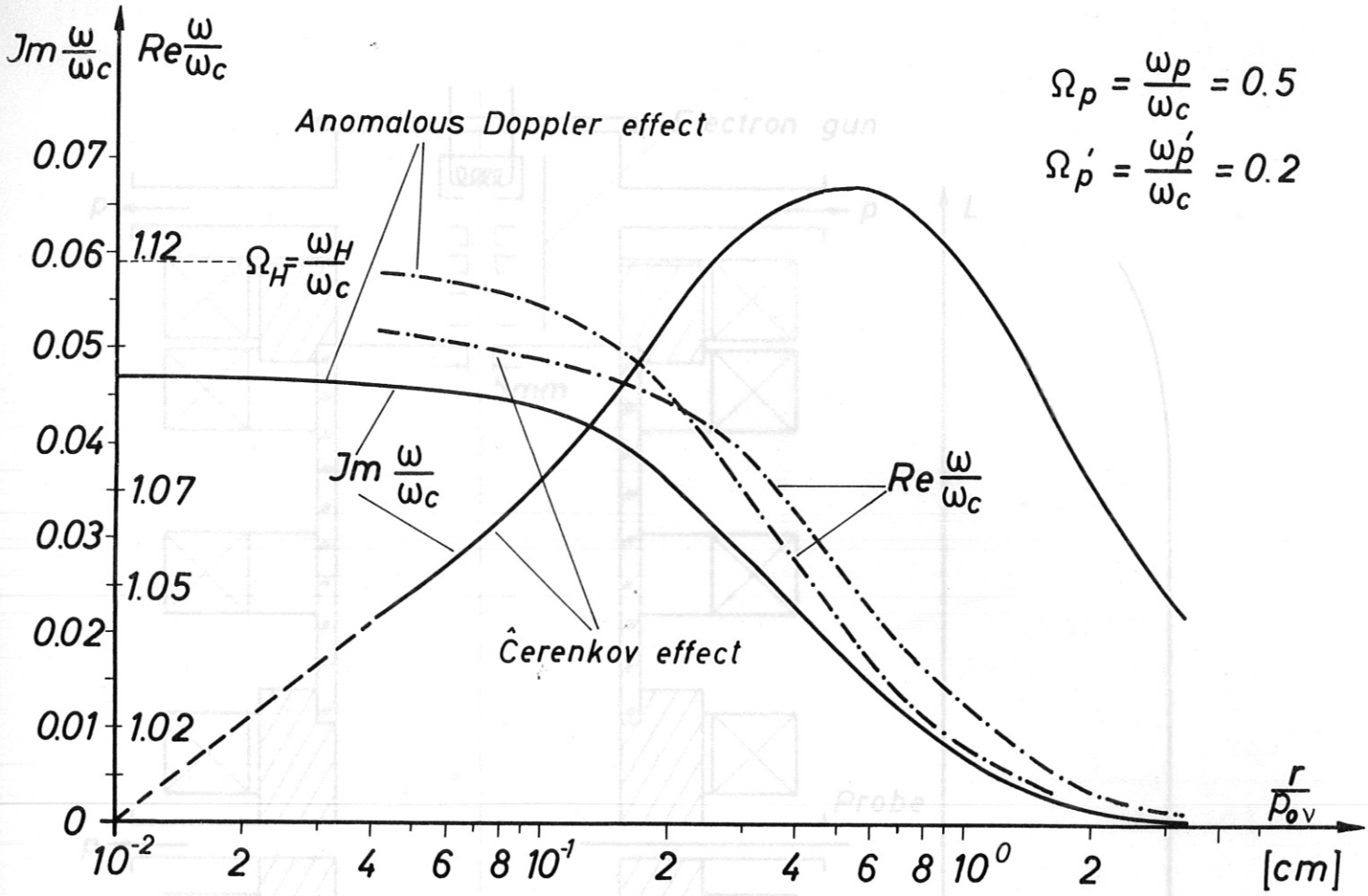
$Jm\frac{\omega}{\omega_c}$
$Re\frac{\omega}{\omega_c}$
$\Omega_p = \frac{\omega_p}{\omega_c} = 0.5$
$\Omega_p' = \frac{\omega_p'}{\omega_c} = 0.2$
Anomalous Doppler effect
0.07
0.06
1.12
$\Omega_H = \frac{\omega_H}{\omega_c}$
0.05
0.04
1.07
0.03
1.05
0.02
0.01
1.02
0
$Jm\frac{\omega}{\omega_c}$
$Re\frac{\omega}{\omega_c}$
Čerenkov effect
$\frac{r}{p_{ov}}$
10^{-2} 2 4 6 8 10^{-1} 2 4 6 8 10^{0} 2
[cm]

Fig. 4

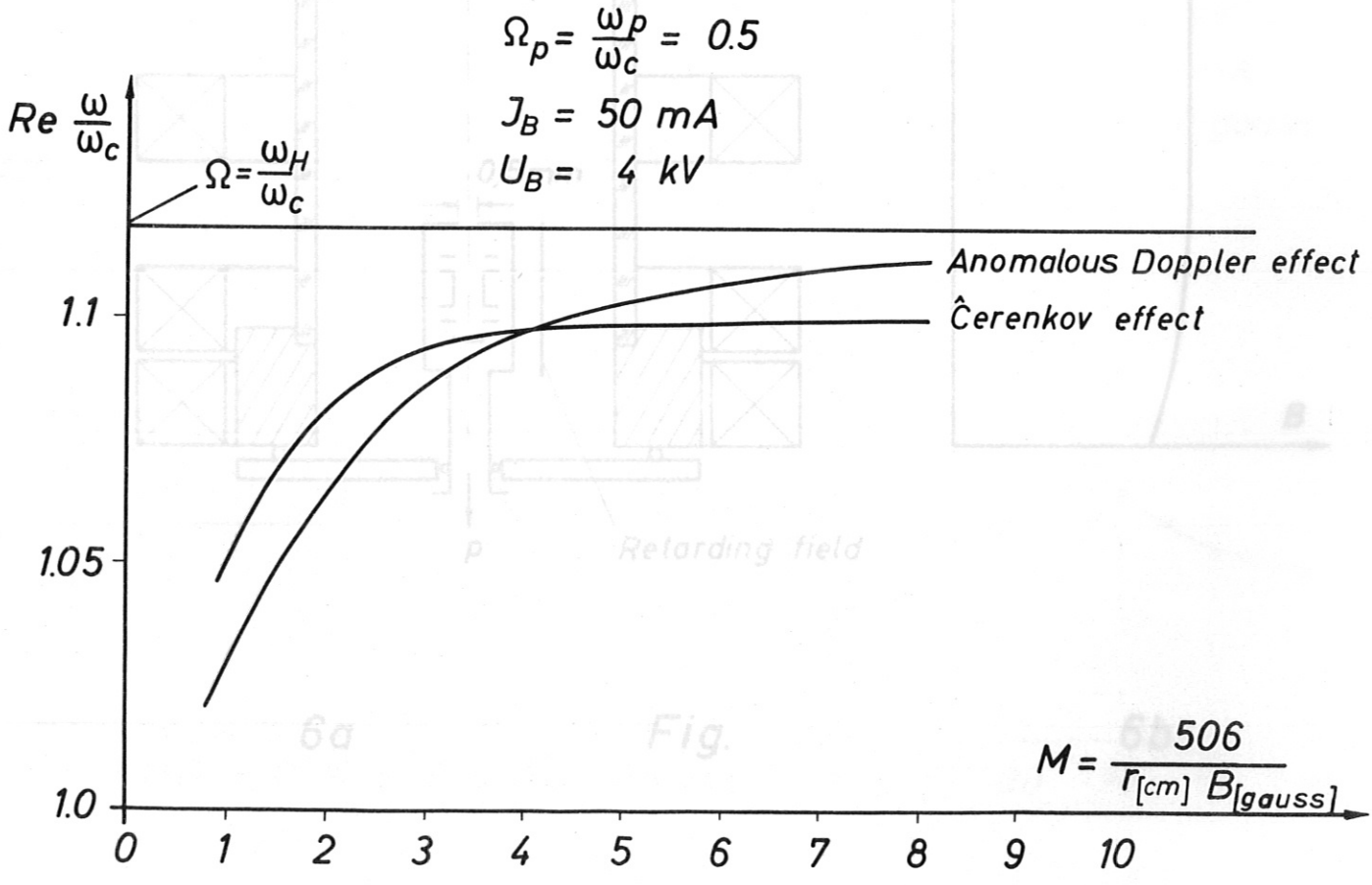
$\Omega_p = \frac{\omega_p}{\omega_c} = 0.5$
$J_B = 50\ mA$
$U_B = 4\ kV$
$Re\frac{\omega}{\omega_c}$
$\Omega = \frac{\omega_H}{\omega_c}$
Anomalous Doppler effect
Čerenkov effect
1.1
1.05
1.0
$M = \frac{506}{r_{[cm]}\ B_{[gauss]}}$
0 1 2 3 4 5 6 7 8 9 10

Fig. 5

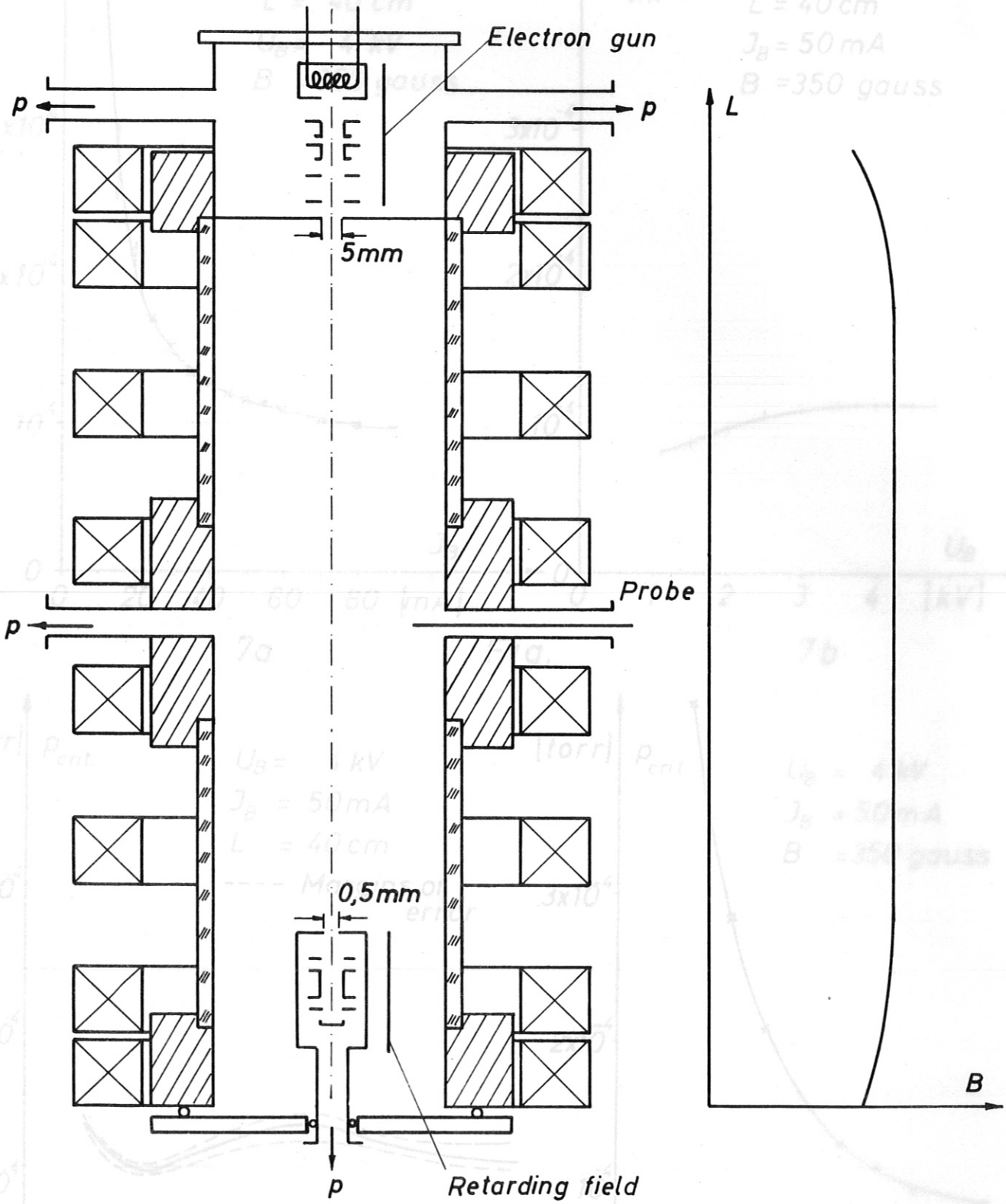

Fig. 6a 6b

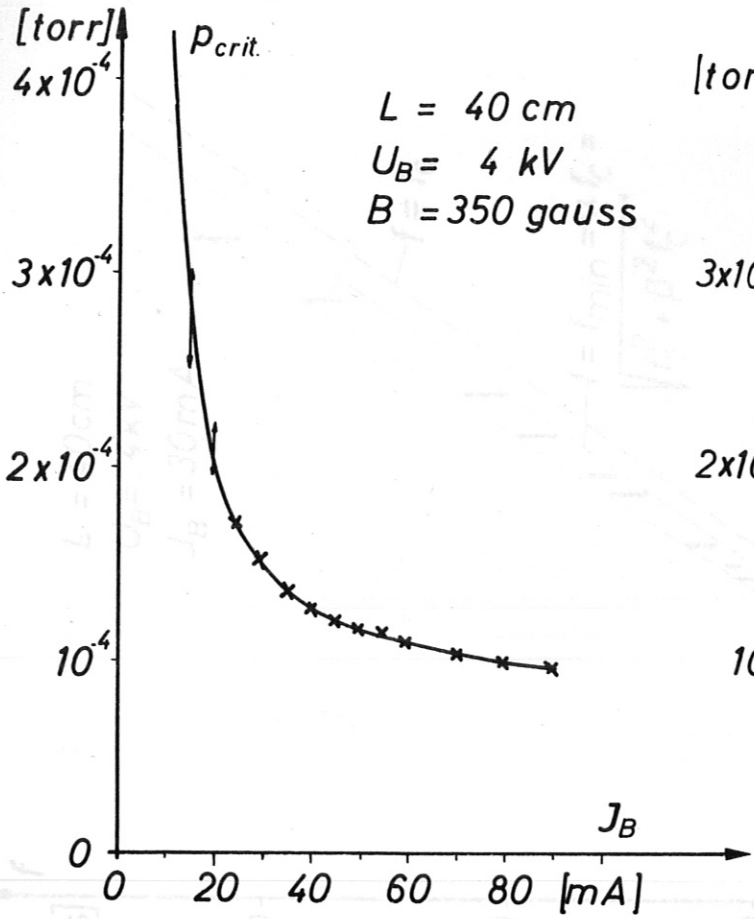

7a

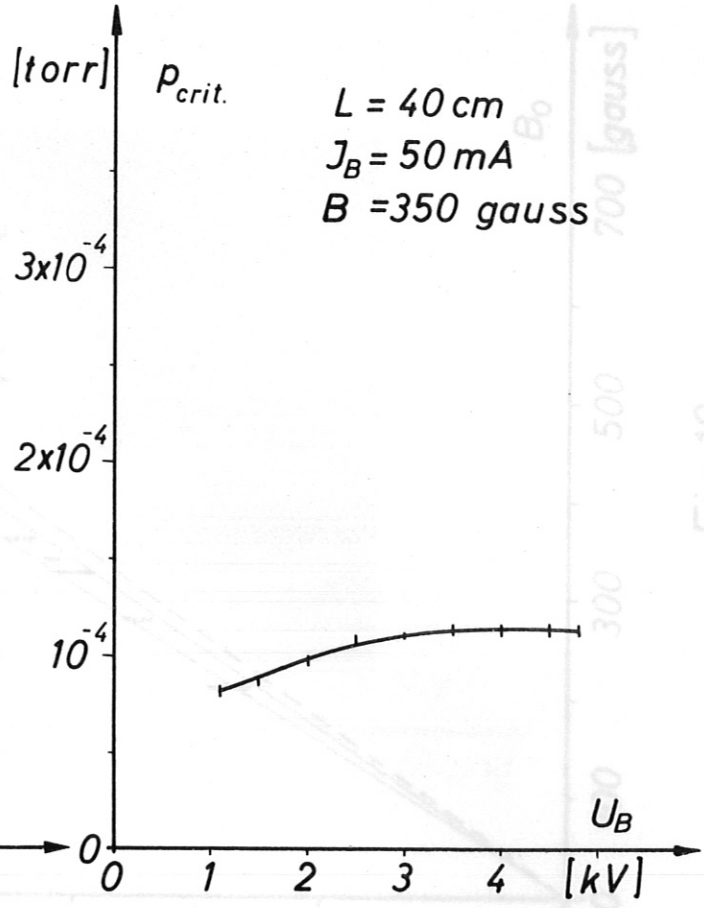

Fig. 7b

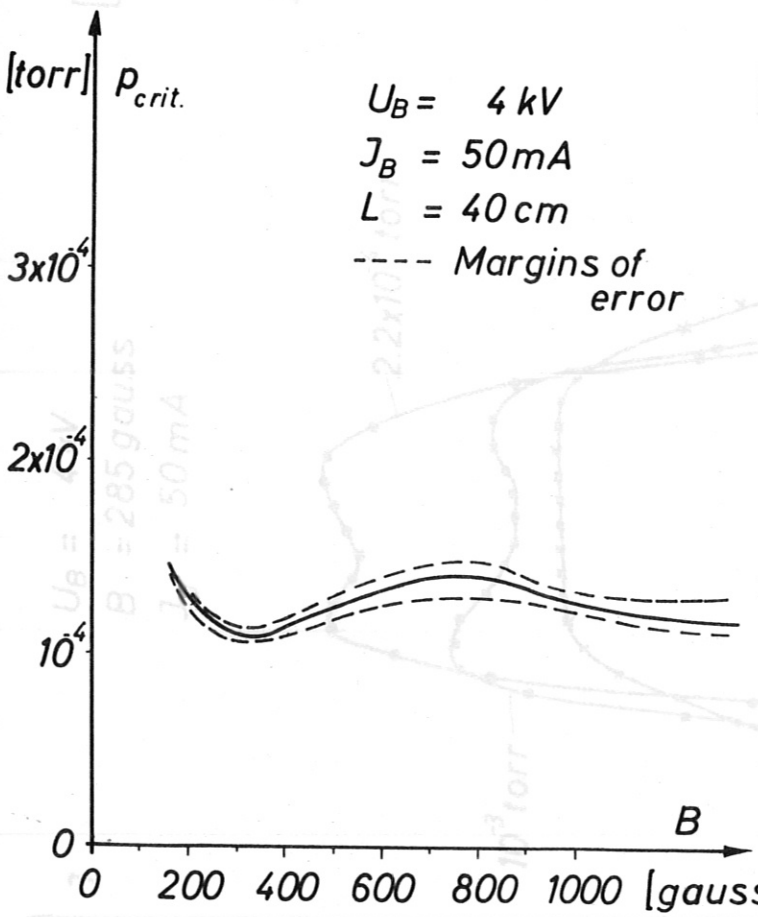

8a

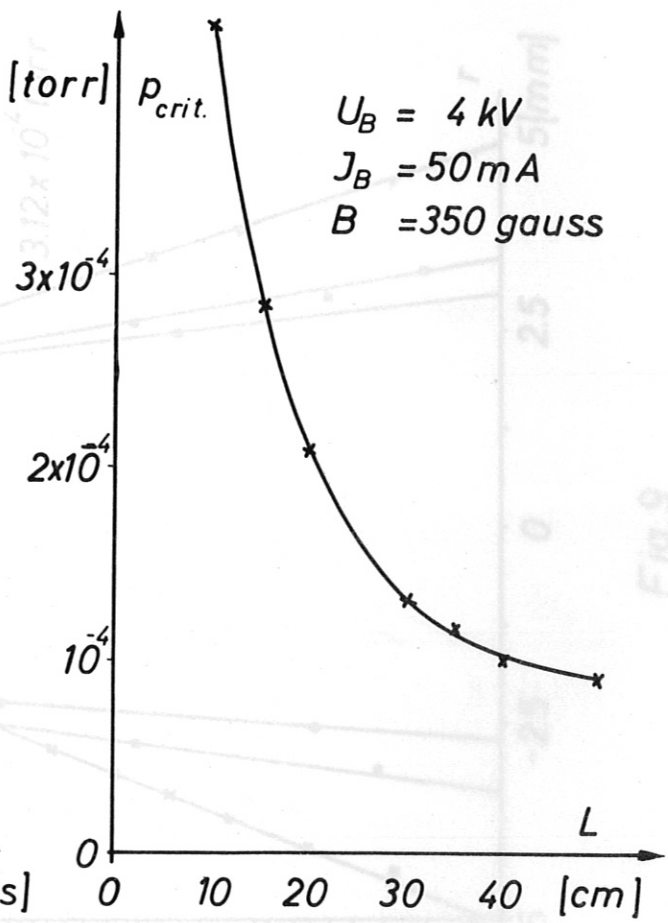

Fig. 8b

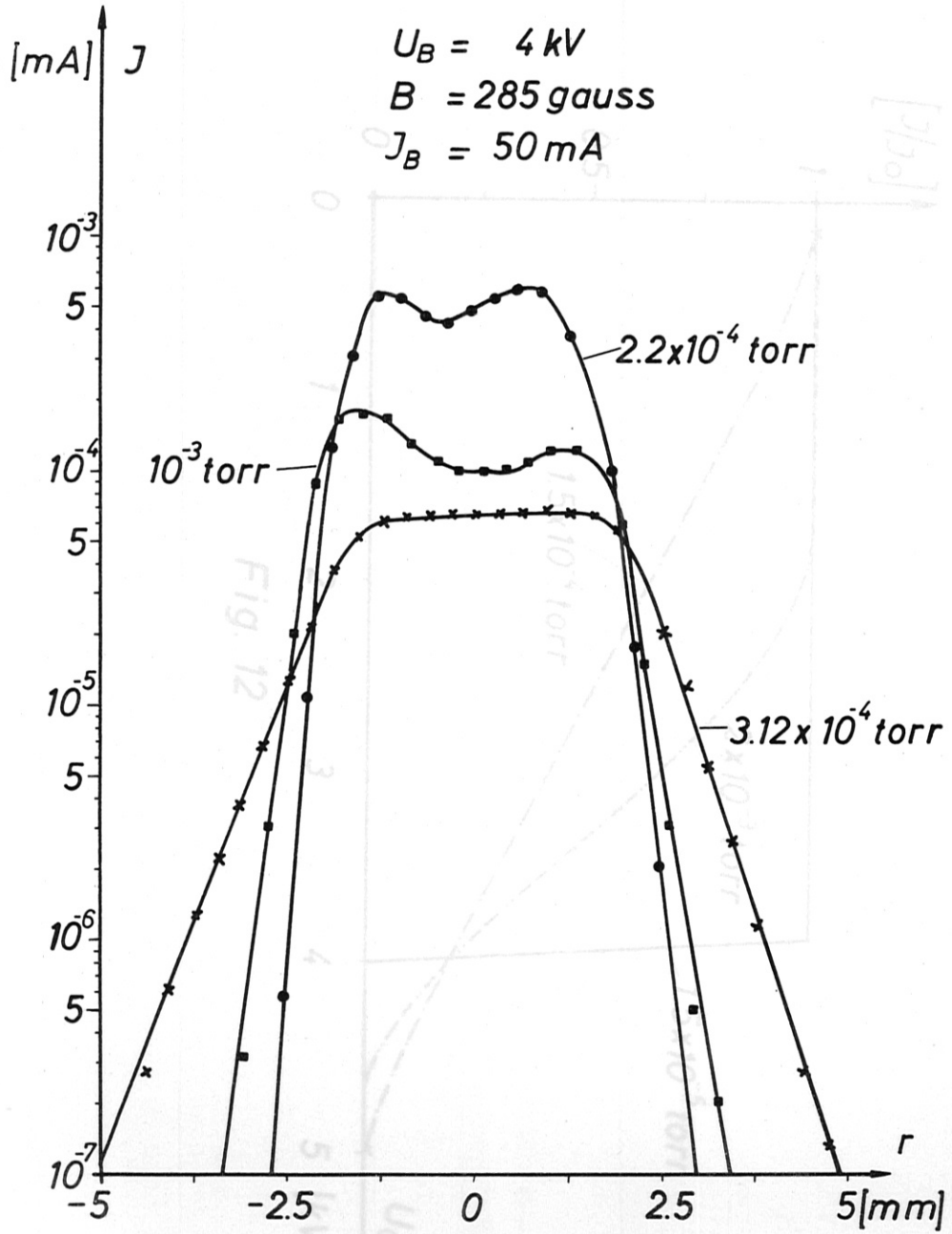
[mA] J
U_B = 4 kV
B = 285 gauss
J_B = 50 mA
10^{-3}
5
10^{-4}
5
10^{-5}
5
10^{-6}
5
10^{-7}
2.2×10^{-4} torr
10^{-3} torr
3.12×10^{-4} torr
r
-5
-2.5
0
2.5
5[mm]

Fig. 9

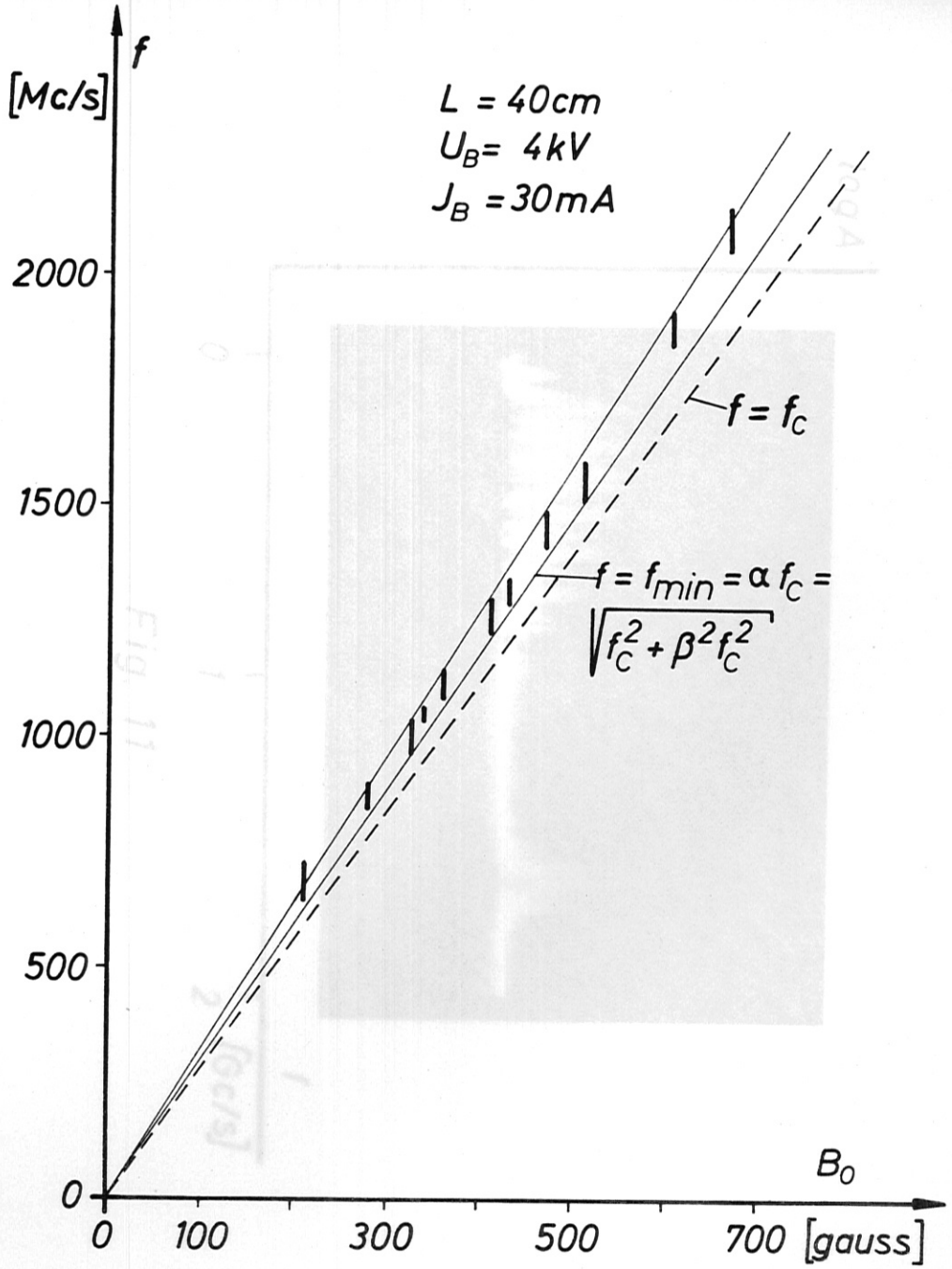
f
[Mc/s]
L = 40cm
U_B = 4kV
J_B = 30mA
2000
1500
1000
500
0
$f = f_C$
$f = f_{min} = \alpha f_C = \sqrt{f_C^2 + \beta^2 f_C^2}$
B_0
0
100
300
500
700 [gauss]

Fig. 10

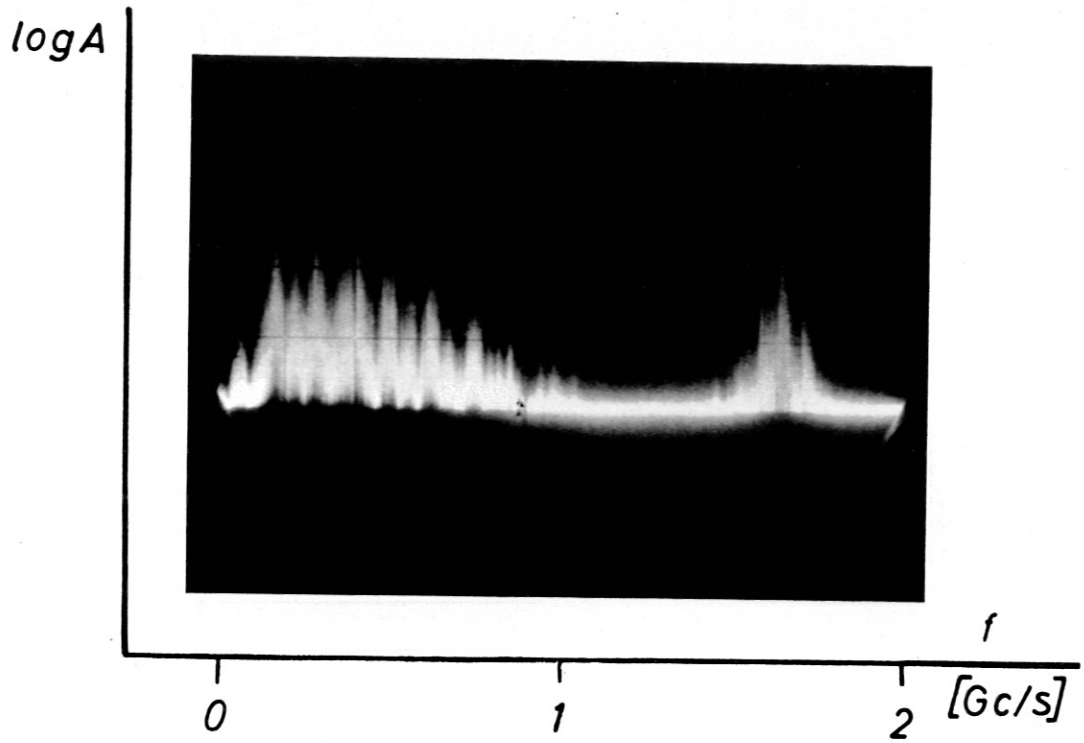
logA
f
0
1
2
[Gc/s]

Fig. 11

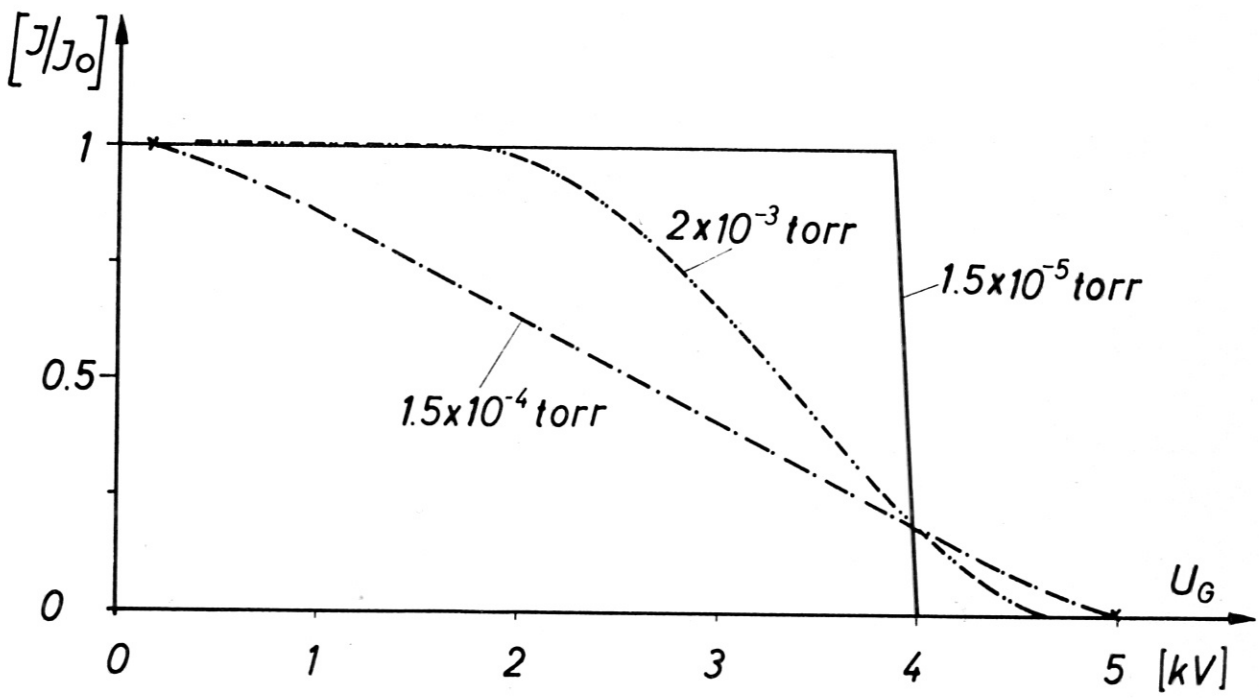
[J/J₀]
1
0.5
0
2x10⁻³ torr
1.5x10⁻⁵ torr
1.5x10⁻⁴ torr
U_G
0
1
2
3
4
5 [kV]

Fig. 12

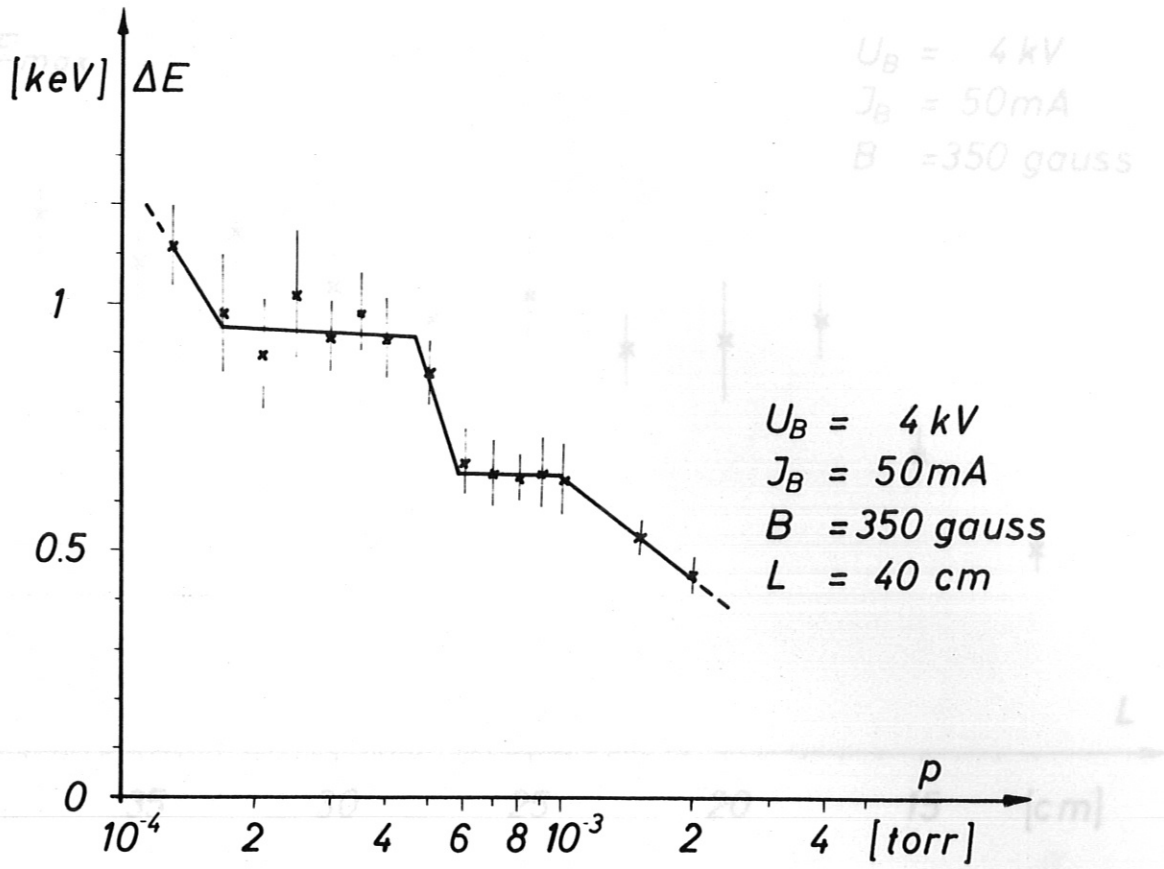
[keV] ΔE
1
0.5
0
U_B = 4 kV
J_B = 50mA
B = 350 gauss
L = 40 cm
p
10^{-4} 2 4 6 8 10^{-3} 2 4 [torr]

Fig. 13

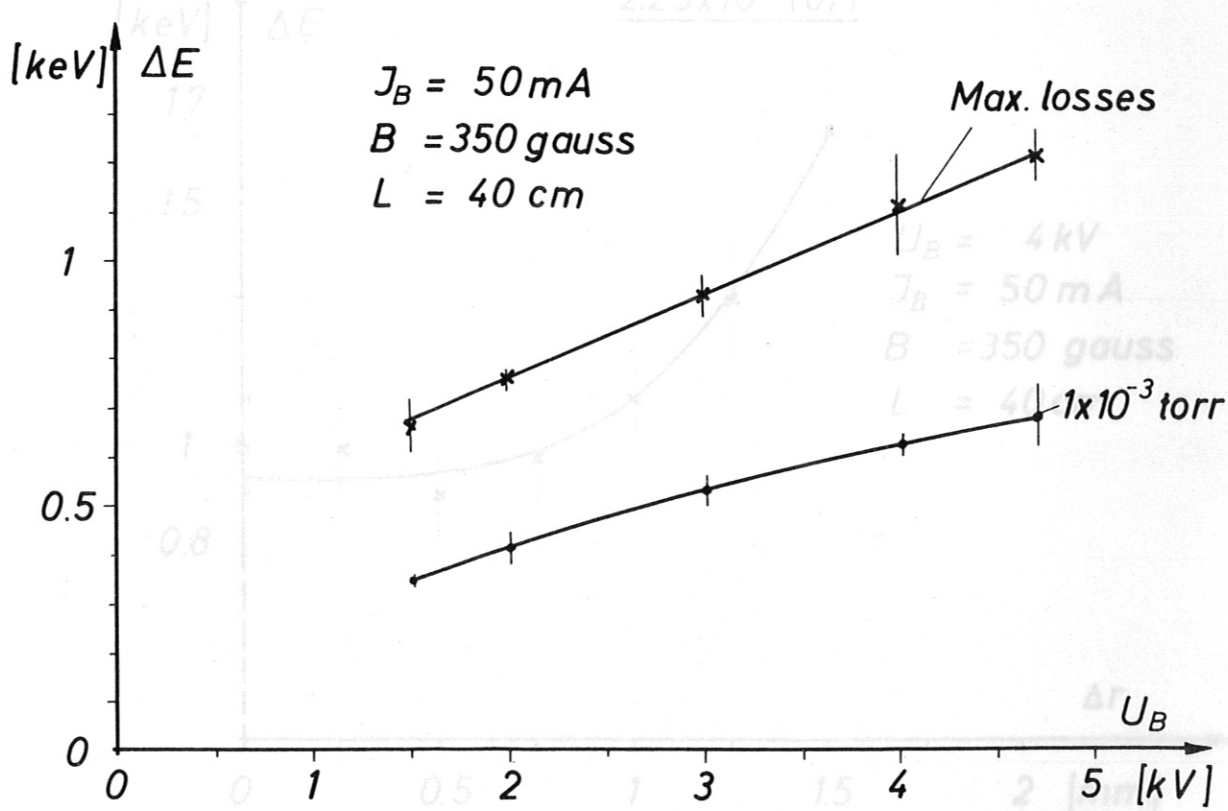
[keV] ΔE
J_B = 50mA
B = 350 gauss
L = 40 cm
Max. losses
$1x10^{-3}$ torr
1
0.5
0
U_B
0 1 2 3 4 5 [kV]

Fig. 14

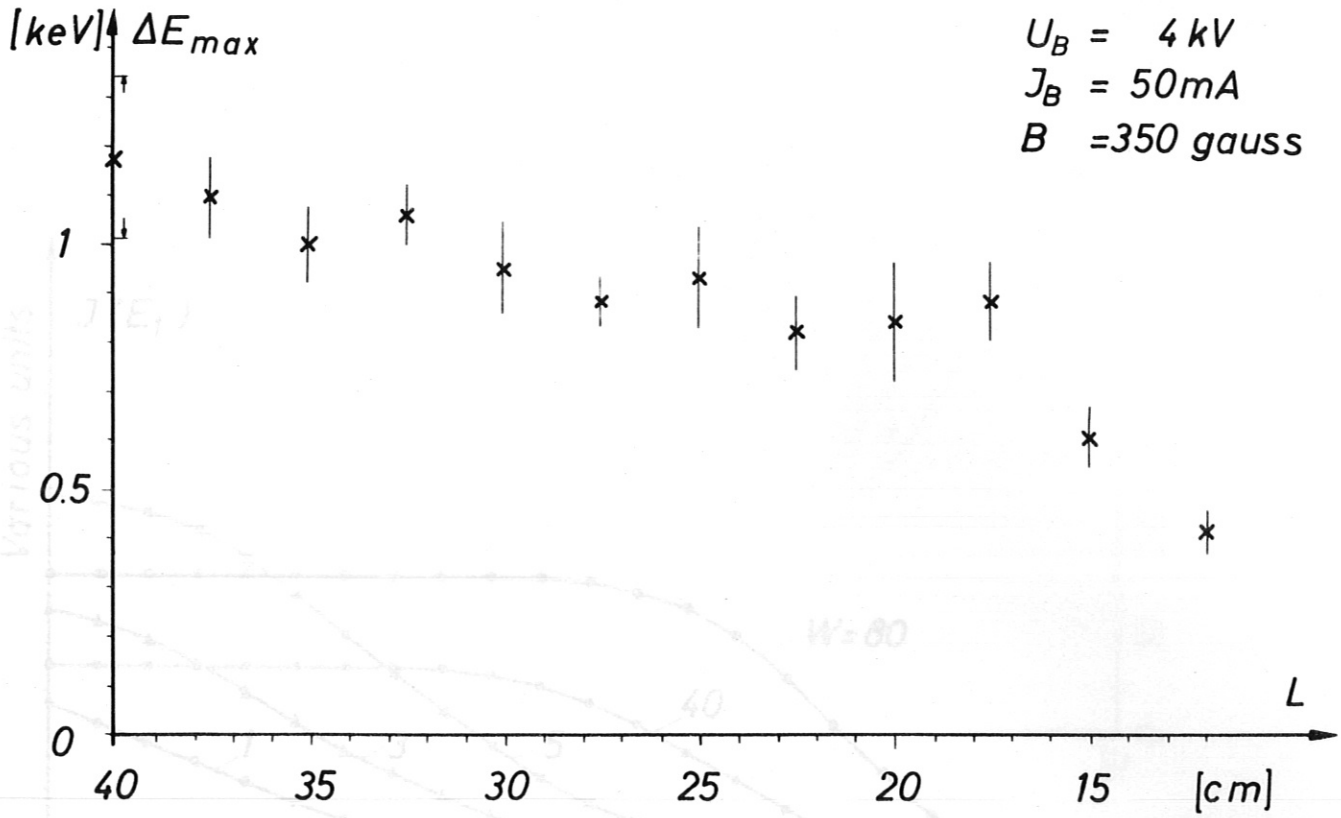
[keV] ΔE max
U_B = 4 kV
J_B = 50mA
B =350 gauss
1
0.5
0
L
40
35
30
25
20
15
[cm]

Fig. 15

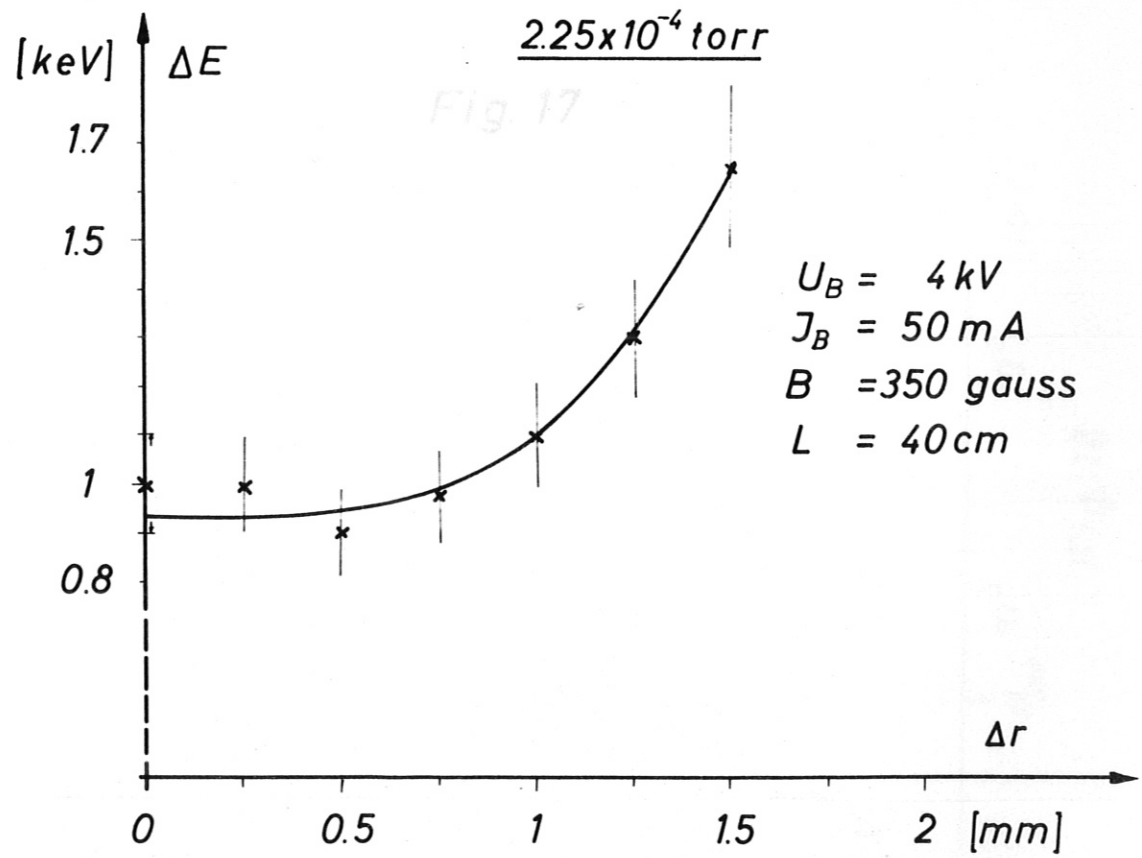
2.25x10⁻⁴ torr
[keV] ΔE
1.7
1.5
1
0.8
U_B = 4 kV
J_B = 50 mA
B =350 gauss
L = 40 cm
Δr
0
0.5
1
1.5
2 [mm]

Fig. 16

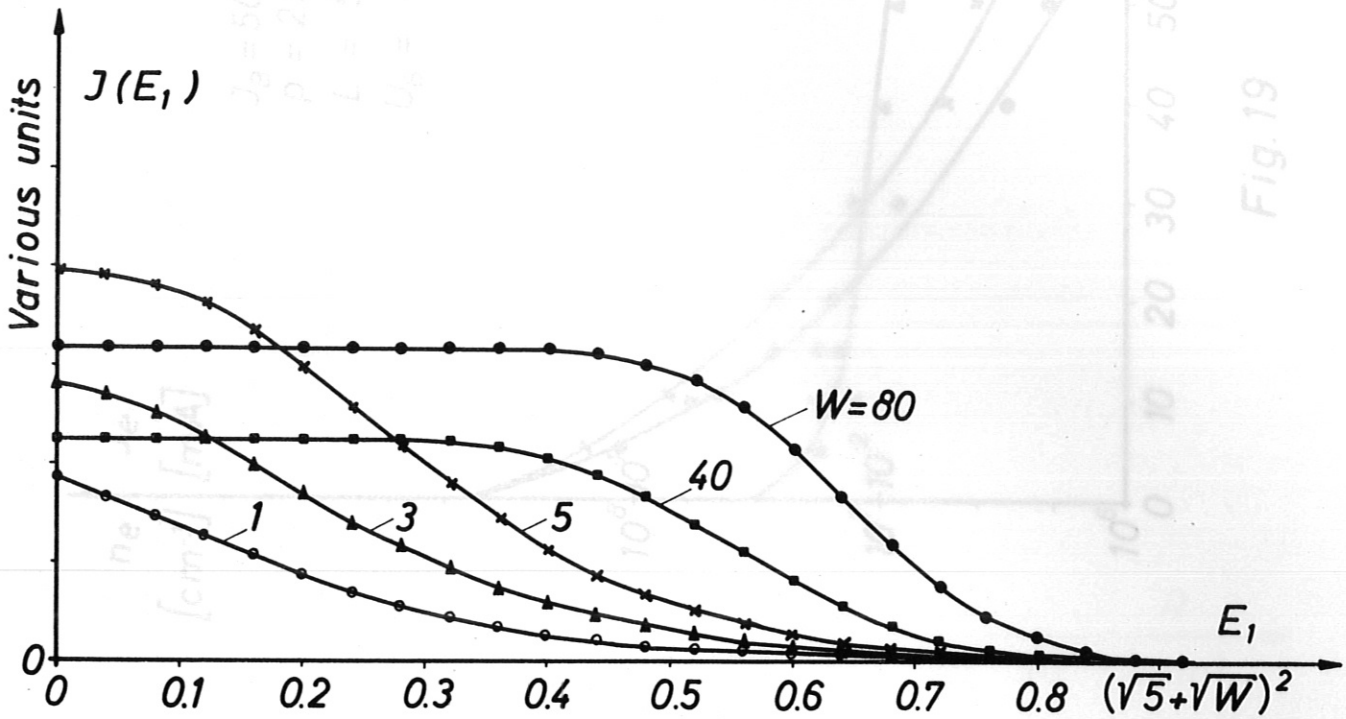

Fig. 17

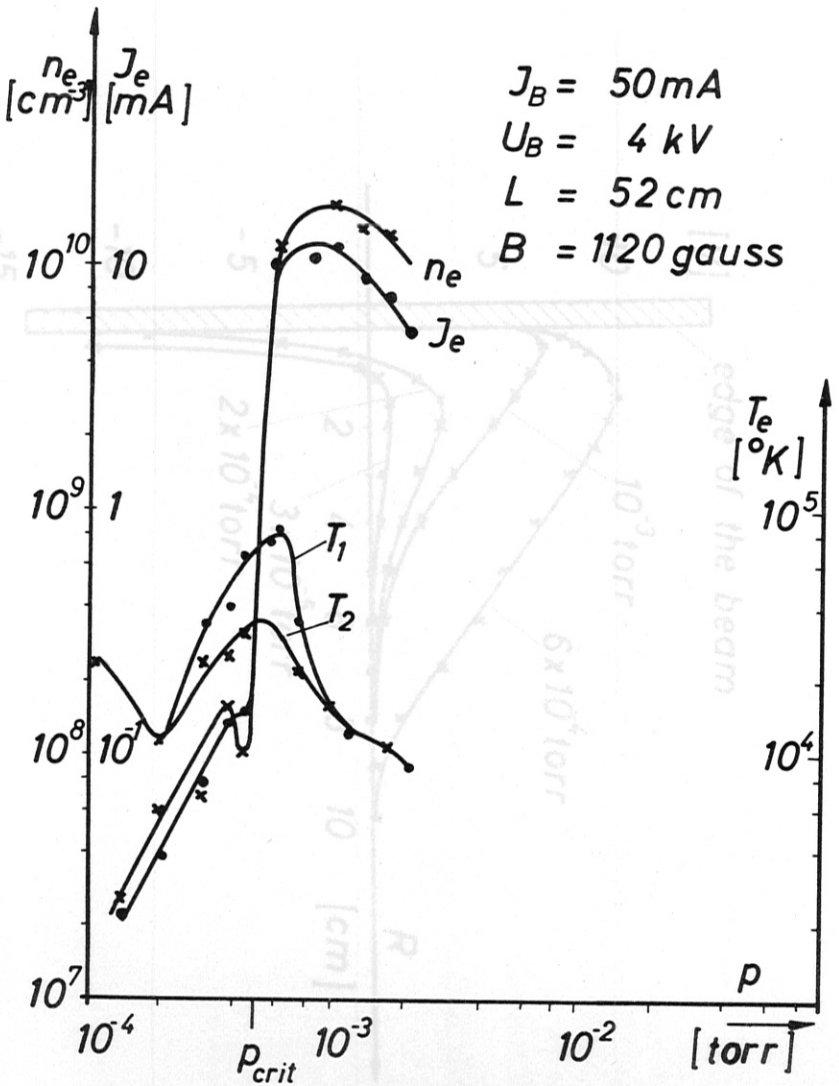
n_e [cm^{-3}]
J_e [mA]
J_B = 50 mA
U_B = 4 kV
L = 52 cm
B = 1120 gauss
10^{10}
10
n_e
J_e
T_e [°K]
10^9
1
10^5
T_1
T_2
10^8
10^{-1}
10^4
10^7
p
10^{-4}
p_{crit}
10^{-3}
10^{-2}
[torr]

Fig. 18

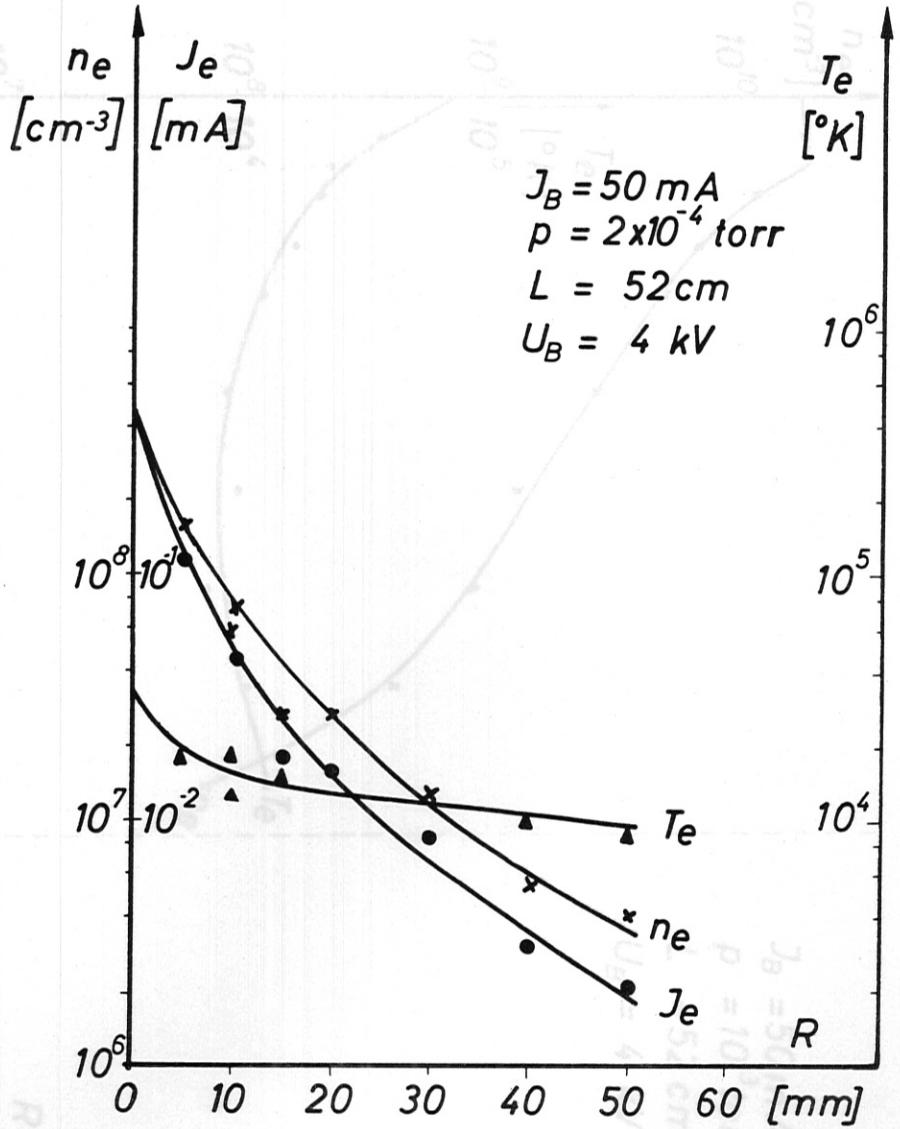
n_e [cm^{-3}]
J_e [mA]
T_e [°K]
J_B = 50 mA
p = 2x10^{-4} torr
L = 52 cm
U_B = 4 kV
10^6
10^8
10^{-1}
10^5
10^7
10^{-2}
10^4
T_e
n_e
J_e
R
0
10
20
30
40
50
60
[mm]

Fig. 19

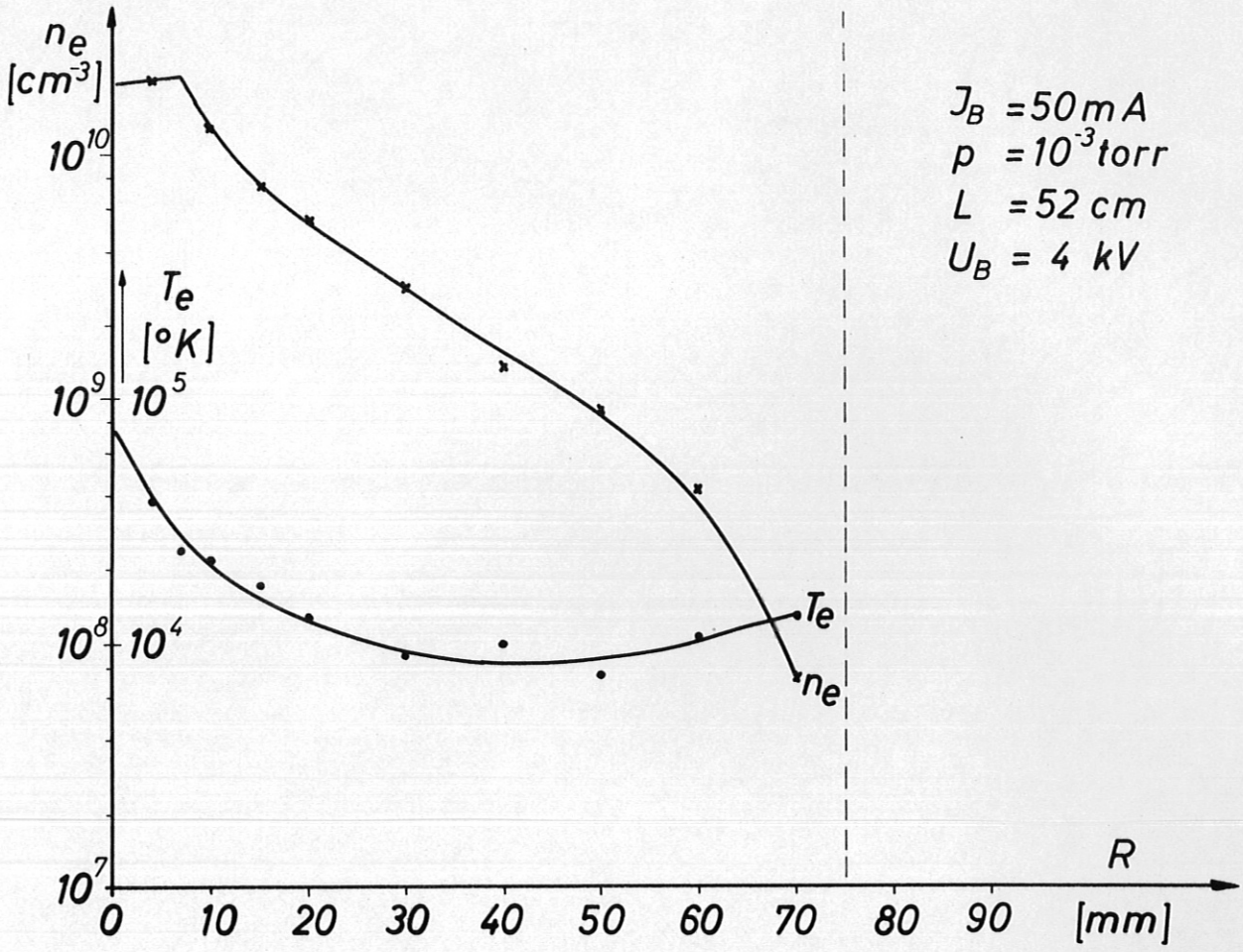
n_e [cm^{-3}]
10^{10}
10^9
10^8
10^7
T_e [°K]
10^5
10^4
T_e
n_e
J_B = 50 mA
p = 10^{-3} torr
L = 52 cm
U_B = 4 kV
R
0 10 20 30 40 50 60 70 80 90 [mm]

Fig. 20

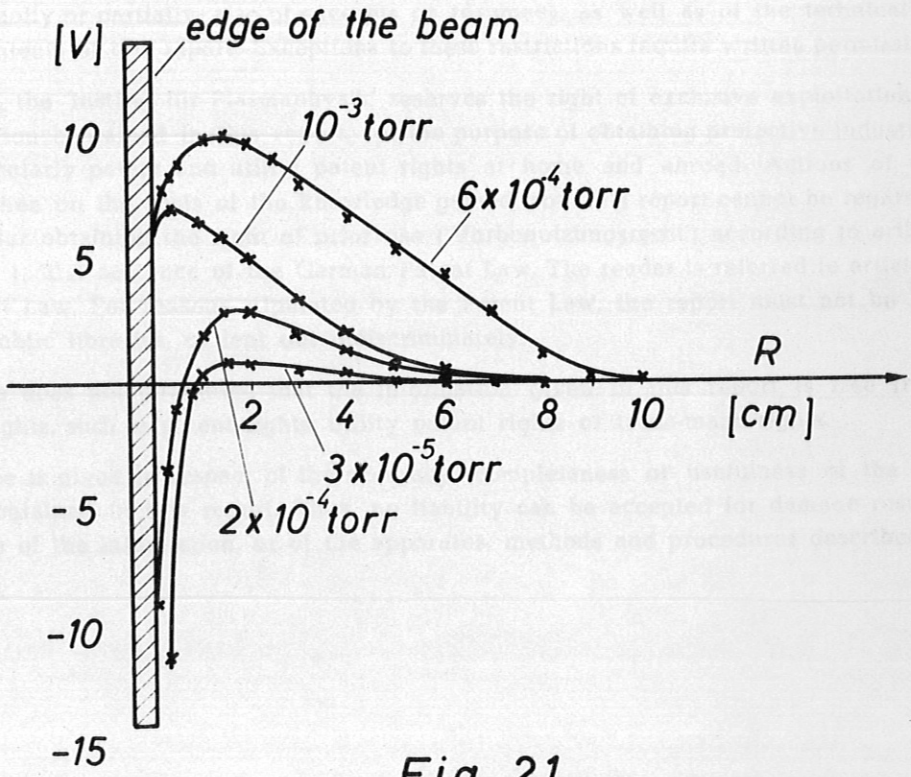
[V]
edge of the beam
10
5
-5
-10
-15
10^{-3} torr
6×10^{-4} torr
3×10^{-5} torr
2×10^{-4} torr
R
2 4 6 8 10 [cm]

Fig. 21